

Block-Fitness Modeling of the Global Air Mobility Network

Giulia Fischetti^{1,+}, Anna Mancini^{2,3,+}, Giulio Cimini^{2,3,4,*}, Jessica T. Davis⁵, Abby Leung⁵, Alessandro Vespignani⁵, and Guido Caldarelli^{1,4,6}

¹DMSN, Ca' Foscari University of Venice, 30172 Mestre (Italy)

²Physics Dept. and INFN, University of Rome Tor Vergata, 00133 Rome (Italy)

³Enrico Fermi Research Center, 00184 Rome (Italy)

⁴CNR-Institute for Complex Systems (ISC), 00185 Rome (Italy)

⁵MOBS Lab, Northeastern University, Boston MA 02115 (USA)

⁶LIMS, Royal Institution, London W1S4BS (United Kingdom)

*giulio.cimini@roma2.infn.it

⁺These authors contributed equally to this work

ABSTRACT

Accurate representations of the World Air Transportation Network (WAN) are fundamental inputs to models of global mobility, epidemic risk, and infrastructure planning. However, high-resolution, real-time data on the WAN are largely commercial and proprietary, therefore often inaccessible to the research community. Here we introduce a generative model of the WAN that treats air travel as a stochastic process within a maximum-entropy framework. The model uses airport-level passenger flows to probabilistically generate connections while preserving traffic volumes across geographic regions. The resulting reconstructed networks reproduce key structural properties of the WAN and enable simulations of dynamic spreading that closely match those obtained using the real network. Our approach provides a scalable, interpretable, and computationally efficient framework for forecasting and policy design in global mobility systems.

Introduction

Statistical physics provides a powerful framework to describe collective behavior in complex systems using limited microscopic information. In recent years, this approach has extended beyond traditional domains to capture socio-economic phenomena, where large-scale patterns emerge from the interactions of many heterogeneous agents^{1–8}. A central example is epidemic spreading, in which the underlying mobility networks shape the pathways of disease transmission^{9–17}. In particular, the World Air Transportation Network (WAN) drives global contagion dynamics by rapidly connecting distant regions^{18–26}. However, despite their central role in computational modeling^{27–29}, high-resolution, near-real-time mobility datasets are frequently unavailable, owing to proprietary ownership, and technical constraints on collection and integration.

Several methods have thus been proposed to infer passenger flows of the global air transportation system, including gravity-based models³⁰, open-access modeled passenger flow matrices^{31,32}, monthly global air travel estimates and, more recently, machine-learning approaches for flight-level traffic forecasting³³. While these methods provide useful approximations of traffic volumes and connectivity patterns, they still suffer from important limitations, such as reliance on incomplete or proprietary data and strong modeling assumptions. A generative framework capable of reproducing the structural and functional properties of the WAN from limited aggregate information is still missing.

Many empirical studies model the WAN as a complex network of airports (nodes) connected by direct flights (links)^{34,35}. Its topology was shown to exhibit a heavy-tailed degree distribution, small-world properties, and a multi-community structure, with dense regional clusters connected by long-range intercontinental routes^{36,37}. Different generative approaches have been developed to capture these features. Preferential attachment processes modulated by geographic distance reproduce the emergence of hubs alongside locally clustered neighborhoods³⁸. Related entropy-based spatial formulations assign link probabilities as functions of node degree and distance, leading to similar macroscopic connectivity patterns^{39–41}. Yet, these approaches largely ignore link weights (traffic volumes), which are not a simple function of connectivity³⁴. Limitations also apply to gravity models, which have long been used to estimate flows between locations based on population and distance^{42–45}, as they inherently produce dense, fully connected systems. This is at odd with the observed sparsity of air networks—arising from operational, economic, and geographical constraints.

Similar challenges arise in other domains where the network structure is only partially observable. In financial and economic systems, for example, regulators often know the aggregate exposures of banks but not the individual connections among

them^{46,47}. Standard reconstruction techniques based on the maximum entropy principle yields fully connected networks, which drastically underestimate systemic risk^{48,49}. To overcome this limitation, improved reconstruction methods have been developed that first infer the existence of links from aggregate exposures according to the *fitness model*^{50,51}, and then assign their weights conditional on those links with a *density-corrected* gravity approach^{52,53}. In this way, they produce sparse weighted networks consistent with prescribed node strengths.

Following this line of research, we propose a generative model of the WAN that reproduces its topology, weights, and spatial organization. We build upon the maximum-entropy framework described above but introduce additional constraints reflecting the modular organization of the air mobility infrastructure^{54,55}. In particular, we partition airports into geographic communities (blocks) and preserve the total flow of passengers among them, while we take passenger traffic at each airport as fitness that drives its connectivity (see Methods for more details). The resulting *block-fitness model*, which represents a natural generalization of the fitness model to spatially embedded networks with community structure, allows the probabilistic generation of synthetic versions of the WAN.

We validate the model output against empirical data and compare with alternative formulations. The model reproduces large-scale spatial patterns driven by geography and inter-regional flows, and accurately recovers network topology and weights of individual connections. When used in metapopulation simulations, the reconstructed networks generate spreading trajectories that closely track those obtained on the empirical WAN, including spatial heterogeneity and timing. The framework remains interpretable and scalable, while retaining analytical tractability, making it suitable for inference and simulation when only partial mobility information is available. Beyond its applications to air transport and epidemic modeling, the approach is applicable to maritime and trade networks, where access to high-resolution mobility data is limited even though aggregate flow information is available.

Results

WAN representation and properties

We consider air-travel data from the Official Aviation Guide (OAG), which reports monthly counts of origin–destination passengers between airports worldwide⁵⁶. We group airports into “basins” by dividing the world into over 3,200 geographic subpopulations that are generated using a Voronoi tessellation of the Earth’s surface, where subpopulations are centered around major transportation hubs (details in Supplementary Materials S1). Passenger flows are then summed across each basin pair. We take the monthly basin networks from September to November, 2019 and compute edge weights by averaging over the number of daily travelers. The resulting network is undirected, with link weight w_{ij} given by the flux of passengers in both directions between basins i and j . For each basin i , the carrying capacity is measured by the strength $s_i = \sum_j w_{ij}$ and the number of connections by the degree $k_i = \sum_j a_{ij}$ ($a_{ij} = 1$ if $w_{ij} > 0$ meaning that i and j are connected, and zero otherwise). Degrees and strengths distributions are well approximated by power-laws with exponential cut-offs⁵⁷, reflecting capacity constraints that limit the number of connections and passengers a single basin can accommodate (Figure 1A). The relation between k and s is sub-linear, with some dispersion (Figure 1B). The distance d_{ij} between basins i and j is computed using the Haversine formula applied to the centroids of the two basins. Links occurrence does depend on geographical distance, as shown by the frequency of connections at different distance intervals (Figure 1C). Basins are partitioned into 11 geographical regions following the prescriptions of the United Nations geoscheme and the World Bank regional classification (Figure 1D). Such partition induces a block structure in the network with very high modularity⁵⁸ (Figure 1E).

Network reconstruction

The central element of our framework is a fitness ansatz, in which node strengths serve as fitness parameters that control expected degrees. This assumption is justified when degrees are strongly correlated with strengths, as is the case for the WAN (Fig. 1B). Consistent with this premise, the model accurately reconstructs node degrees as ensemble expectations (Fig. 2A). Node strengths, by contrast, are reproduced by construction (Supplementary Materials S2).

Concerning the inference of individual links, we measure the empirical link probability as a function of the model link probability p_{ij} , by binning p_{ij} values and counting the fraction of linked (i, j) pairs in each bin. We obtain a very good agreement between the two quantities (Figure 2B). Besides, the model recovers very well the weights of existing WAN connections, as ensemble averages $\langle w_{ij} \rangle$ (Figure 2C).

We further employ the model link probability to determine the outcome of a binary classification test on the existence of a link—the well-known task of *link prediction*. A link that exist in the data, $a_{ij} = 1$, is predicted by the model with probability p_{ij} , counting as a True Positive. Note that values of *Precision* ($\sum_{ij} a_{ij} p_{ij} / \sum_{ij} p_{ij}$) and *Recall* ($\sum_{ij} a_{ij} p_{ij} / \sum_{ij} a_{ij}$) of the classifier are equal in our case, since by construction model networks have on average the same number of links of the empirical one (see Methods). We obtain a very high precision of 75%, meaning that the model is able to correctly guess three over four of the existing links (on average over the model ensemble). This result is remarkable in light of the low density of the network (1.8%,

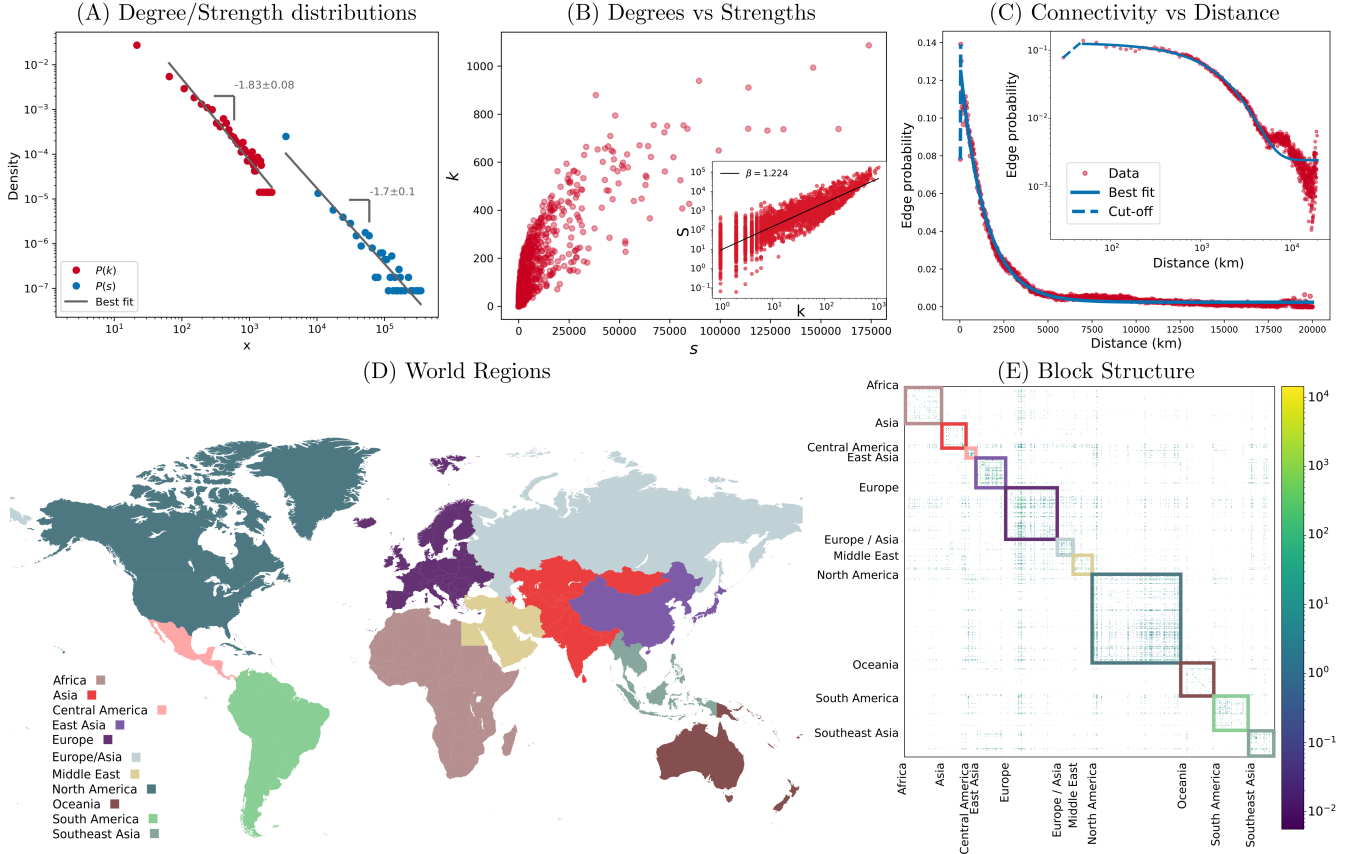


Figure 1. Topological features of the WAN. (A) Degree distribution with power-law fit $P(k) \sim k^{-\gamma_k}$ and exponent $\gamma_k = 1.8(3)$, and strength distribution with power-law fit $P(s) \sim s^{-\gamma_s}$ and exponent $\gamma_s = 1.(7)$. (B) Degree-strength relation, with OLS fit $s \sim k^\beta$ and exponent $\beta = 1.2(2)$. (C) Link probability as a function of geographic distance. The curve is fitted with a linear function $l(d) = m \cdot d + q$ up to a characteristic distance $d^* = 50\text{km}$ and then with an exponential $l(d) = \exp[-a(d - d_0)] + b$. Best fit parameters are $m = 0.003$, $q = -0.0013$ for the linear term and $d_0 = -2.(9) \cdot 10^3$, $a = 7.(1) \cdot 10^{-4}$, $b = -2.(4) \cdot 10^{-3}$ for the exponential decay ($R^2 = 0.99$). (D) World partition into regions: Africa, Asia, Central America, East Asia, Europe, Europe/Asia, Middle East, North America, Oceania, South America, Southeast Asia. (E) Community structure in the WAN adjacency matrix induced by the world partition, with modularity $M = 0.67$.

corresponding to the precision of a random classifier): the dataset is highly unbalanced, with only a few “positives” existing links that are very difficult to guess.

The model can also reconstruct the signature properties of the WAN. It captures the trend and the full dispersion of the k vs s relation (Figure 2D). It reproduces, to a large extent, the dependence of link occurrence on geographic distance (Fig. 2E), despite not using any explicit spatial information. By construction, it recovers the network’s block structure (Fig. 2F).

Spreading simulations

Finally we test the block-fitness model on reproducing results of epidemic simulations on the real network. We use a stochastic metapopulation model for global epidemic spreading, where the epidemic compartmental equations in each basin are coupled through the passenger flows set by the WAN travel matrix⁹ (see Methods for further details). Figure 3 illustrates the spatiotemporal dynamics of contagion on both the real and model WAN, for a representative case in which the epidemic outbreak originates in London. Prevalence maps (Fig. 3A and Fig. 3B for the real and model networks, respectively) show the global distribution of basin-level prevalence $i_m(t)$ at a fixed time, where $i_m(t)$ denotes the fraction of infected individuals in basin m at time t relative to its total population. The temporal evolution of the total prevalence $i(t)$ —defined as the fraction of infected individuals worldwide (Fig. 3C)—exhibits the characteristic epidemic peak. To quantify the spatial heterogeneity in disease prevalence, we compute the normalized spatial distribution $\rho_m(t) = i_m(t) / \sum_n i_n(t)$ and its associated entropy $H(t) \propto \sum_m \rho_m(t) \log \rho_m(t)$. This quantity vanishes when the epidemic is fully localized within a single basin and is maximized when the epidemic is homogeneously spread across the globe²¹ (a condition that typically occurs in correspondence

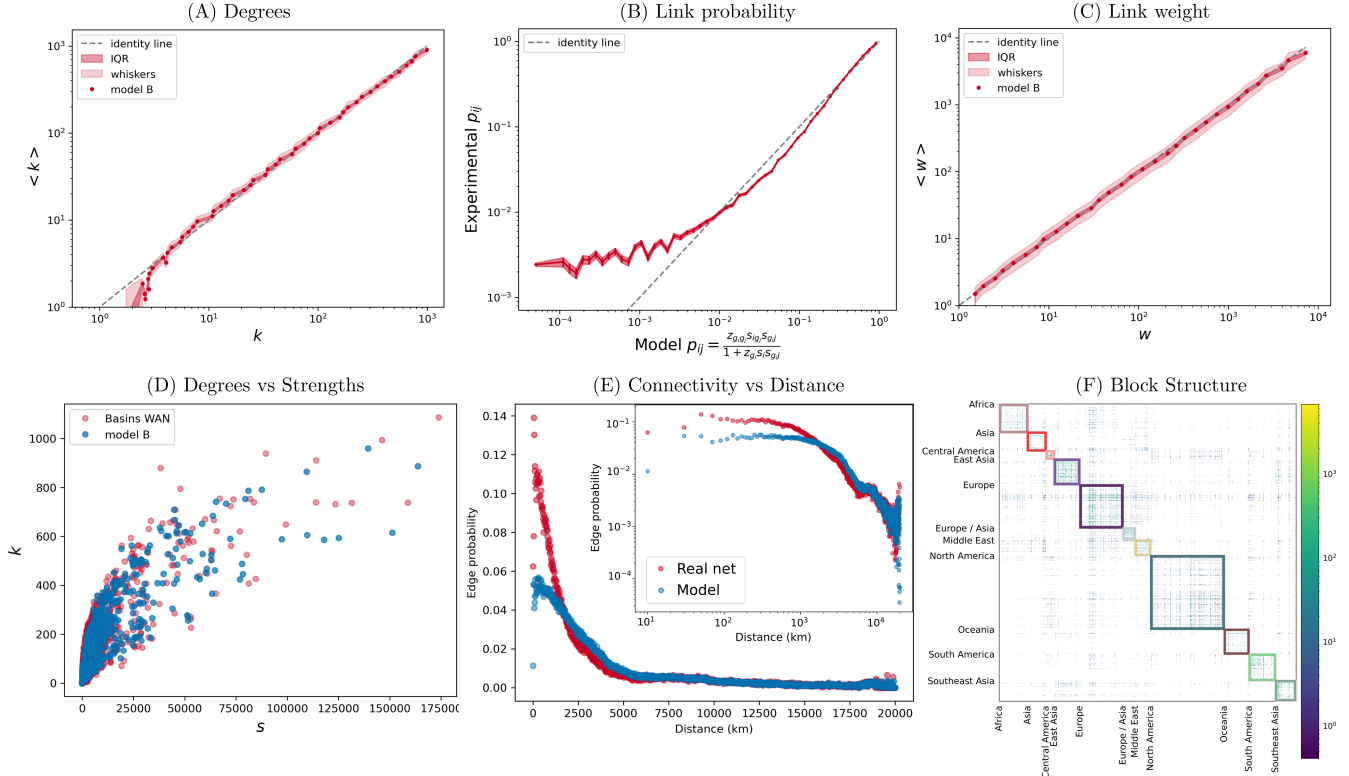


Figure 2. Reconstruction of the topological properties of the WAN. (A): Model degrees $\langle k_i \rangle = \sum_{j \neq i} p_{ij}$ versus empirical degrees k_i , with Root Mean Squared Percentage Error (RMSRE) equal to 0.18. (B): Empirical link probability (given by the fraction f_{ij} of ij pairs that are actually connected in each bin of p_{ij}) as a function of the model link probability p_{ij} , with RMSRE = 0.016. (C): Average model weights $\langle w \rangle_{ij}$ versus empirical weights w_{ij} , with RMSRE = 0.063. For this exercise, we limit the test set to links $w_{ij} > 0$ that are actually realized. For (A,B,C), the dashed identity line marks the perfect agreement between empirical and model values, while the shaded regions represent the inter-quartile range and the whiskers of the set of model values. (D) Degrees vs Strengths relation, with OLS fit exponent $\beta = 1.2(2)$ on empirical data and $\beta = 1.17(0)$ on model data. (E) Link probability as a function of distance, with Mean Squared Error (MSE) between empirical and model curve of 2.21. (F) Block structure of a sample reconstructed network. Modularity is 0.63 on average over the model ensemble (to be compared with $M = 0.67$ for real data).

of the epidemic peak, Fig. 3D).

While visual comparison reveals very few differences between contagion dynamics on real and model networks (the prevalence maps and the epidemic peak are very well reproduced), we consider several complementary metrics to quantitatively compare simulations on real and model WAN. We measure the overall mismatch between the prevalence curves using the area between curves and their L2 distance, while we capture differences in outbreak timing, intensity and duration by measuring the difference in peak time, peak magnitude and epidemic length. Further we compute the Root Mean Square Error (RMSE) of the basin-level prevalence values $i_m(t)$, averaged over time, and the L2 distance between the entropy curves. Table 1 reports values of these quantities, averaged over several simulations on empirical or model networks. Note that we always compare simulations with the same initial seed, but we average across various seeds to evaluate model performance across multiple starting points of the dynamics (which should not influence model performance). We obtain very low values for all metrics that, notably, are very close to the values computed only among simulations on the real network, thus quantifying the intrinsic variability of the dynamics. Overall, the epidemic spreading patterns on the model network closely follow those observed on the real WAN.

Discussion

In this paper we introduced a maximum-entropy framework to model the global air mobility network, which uses airport passenger capacity as fitness to determine connectivity, while preserving passenger fluxes among geographic communities. The model is able to faithfully reconstruct the network features of the WAN, the presence and weight of individual connections

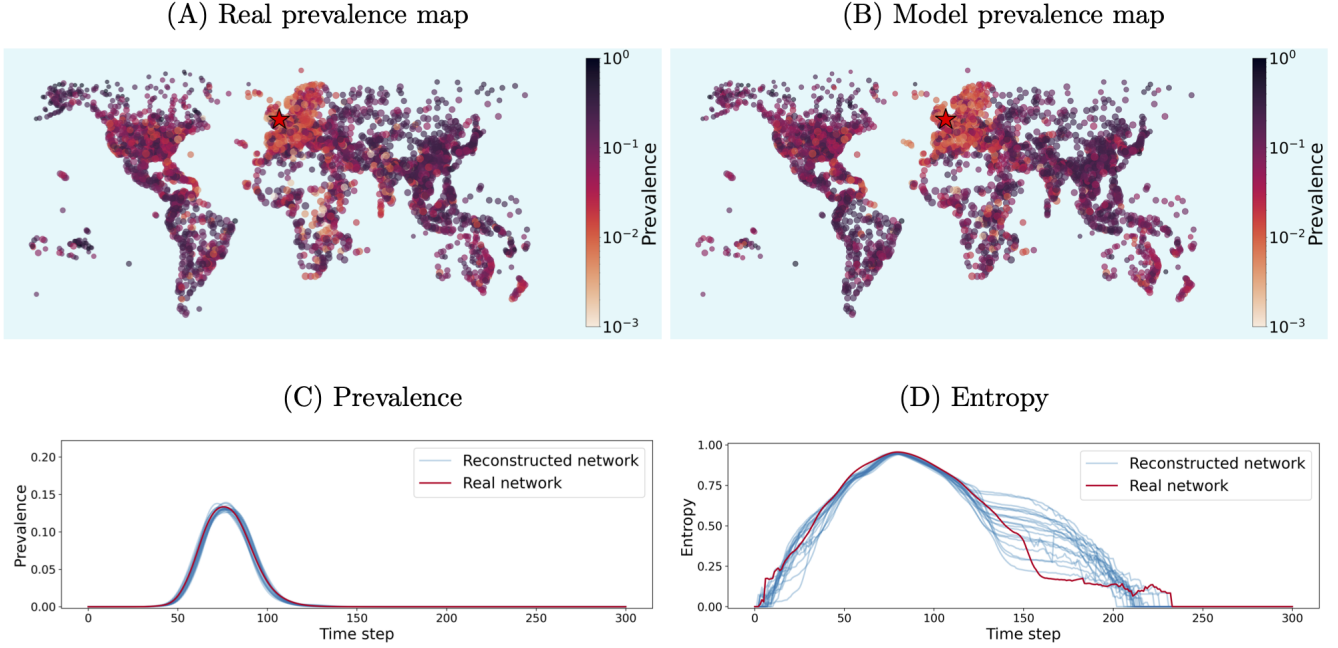


Figure 3. Epidemic simulations starting from London. Prevalence map at simulation step $t = 80$ for the empirical (A) and model (B) WAN. Time evolution of the prevalence (total fraction of infected individuals) (C) and of the entropy of the prevalence distribution (D), for one real simulation and 20 model simulations.

	Δ area	$L2[i]$	Peak time	Peak magn.	Epid. length	$RMSE[i_m]$	$L2[H]$
Model	0.56 ± 0.31	0.073 ± 0.040	2.3 ± 1.8	0.0048 ± 0.0035	4.5 ± 3.2	0.050 ± 0.006	14 ± 6
Data	0.43 ± 0.32	0.058 ± 0.042	2.0 ± 1.7	0.0043 ± 0.0034	2.2 ± 2.2	0.024 ± 0.005	13 ± 6

Table 1. Similarity of epidemic simulations on real and model networks, in terms of: area between and $L2$ distance of prevalence curves; differences of peak time, peak magnitude, epidemic length; RMSE of prevalence vectors; $L2$ distance of entropy curves (definitions in Supplementary Table S3). Values on the “model” row are averages over pairwise comparisons of one simulation on the empirical network and one simulation on a model network, while “Data” values are computed with simulations on the empirical network only. Uncertainties are given as standard deviations.

(achieving a link prediction precision of 75%), as well as the dynamical patterns of epidemic spreading. The block-fitness approach outperforms alternative model formulations, incorporating the super-linear relation between strengths and degrees³⁴ and the dependency of connection probabilities on the geographical distance⁴⁰ (see Supplementary Materials S2 for model definitions and Supplementary Materials S3 for model comparison). Our results are confirmed also if we consider global air mobility at a finer geographical scale than metropolitan areas, where nodes correspond to individual airports (results reported in Supplementary Materials S4).

The community partition is specified a priori using the UN geoscheme and World Bank regional classification, rather than inferred from the network data. Accordingly, we do not optimize the reconstruction with respect to the chosen partition, and a data-driven refinement of the community structure could further improve performance. Future work may also develop extensions in which binary and weighted constraints jointly inform the reconstruction, or in which the observed topology is used as prior information for weight assignment^{59,60}. These variants could then be evaluated for their ability to reproduce the features of more realistic dynamical models. Note also that our inference framework is fully model-based (*white-box*): We do not compare against *black-box* machine learning methods, which can improve results at the cost of interpretability and generalizability. Our model is able to reconstruct the network from aggregate information without training on real instances, i.e, without *ever seeing the full network*. The results provided here indicate that combining degree–strength constraints with coarse-grained spatial organization can be used to generate realistic WAN surrogates for forecasting and policy analysis.

Methods

Model formulation

Our modeling approach belongs to the class of Exponential Random Graphs (ERGs)^{39,61–63}, which builds on the principle of Maximum Entropy⁶⁴ to generate ensembles of networks that are maximally random but preserve, on average, some features of the empirical network^{7,65,66}. This recipe allows obtaining the most unbiased probability distribution describing a network with the imposed features, while model parameters can be efficiently obtained with scalable algorithms⁶⁷. For this approach to work in the context of sparse weighted complex networks (the typical situation encountered in real case scenarios), the features to be imposed are both node strengths and degrees^{59,68}. Indeed, without constraining degrees, the generated network would be fully connected, because strengths alone do not contain information on how many links should be actually realized (see the *irreducibility conjecture* in⁶⁹): unconstrained entropy maximization distributes the available weight over all possible (in fact all) connections. In the common situation where degree information is not available, a heuristic *fitness ansatz*⁵⁰ can be used to replace the corresponding model parameters with other node properties that are positively correlated with the degree – typically, the strengths themselves⁵¹. The underlying natural assumption is that nodes with large strength are likely to be connected. The model can then be formulated as a two-step inference procedure^{52,69}, where links are first sampled independently according to a connection probability that depends on node strengths, and then assigned a weight according to a *corrected gravity model* prescription. This recipe thus generates sparse topologies while preserving node strengths.

Here we build on this formulation by imposing a community structure on the model network while keeping the global strength constraints. We thus split nodes into a set $\{g\}$ of communities and, for each node i , we constrain the strength values computed with respect to each community g : $s_{ig} = \sum_{j(\neq i) \in g} w_{ij}$. The probability of connection for nodes i and j (with $i \neq j$), belonging respectively to community g_i and g_j , thus reads:

$$p_{ij} = \frac{z_{g_i g_j} s_{ig_j} s_{jg_i}}{1 + z_{g_i g_j} s_{ig_j} s_{jg_i}}$$

which depends on s_{ig_j} and s_{jg_i} (the required inputs of the model). The free parameter $z_{g_i g_j}$ is determined by setting the expected number of connections among communities g_i, g_j equal to the empirical value: $\sum_{i \in g_i} \sum_{j \in g_j} p_{ij} = \sum_{i \in g_i} \sum_{j \in g_j} a_{ij}$ (details in Supplementary Materials S2). Then, each sampled link ij (realized with probability p_{ij}) is assigned the weight:

$$w_{ij} = \frac{s_{ig_j} s_{g_i j}}{p_{ij} W_{g_i g_j}}$$

while $w_{ij} = 0$ otherwise. $W_{g_i g_j} = \sum_{i \in g_i} \sum_{j \in g_j} w_{ij}$ is the total weight of connections among nodes in g_i and g_j . The average link weight thus reads $\langle w_{ij} \rangle = s_{ig_j} s_{g_i j} / W_{g_i g_j}$, hence the model preserves, as ensemble averages, the strength by block of each node: $\langle s_{ig_j} \rangle = \sum_{j \in g_j} \langle w_{ij} \rangle \equiv s_{ig_j}$ (and thus the total strength). This model formulation can be seen as a composition of fitness models for each block⁶⁹ or as a fitness-based version of discrete latent variable models^{54,55}. We report in the Supplementary Materials S2 the the model formulation for directed networks.

Epidemic simulations

We implement metapopulation simulations of epidemic spreading across the WAN by coupling a Susceptible-Infected-Recovered (SIR) dynamics taking place in each basin with mobility among different basins according to the WAN^{9,70}. To do so we use the *Epidemiology 101* package⁷¹, available at <https://github.com/DataForScience/Epidemiology101/tree/master>. For each basin m , the number of susceptible, infected and recovered individuals, denoted S_m , I_m , and R_m (with $S_m + I_m + R_m = N_m$ the total population m), evolves according to a stochastic SIR dynamics, described by the mean-field equations

$$\left\{ \begin{array}{l} \frac{dS_m}{dt} = -\frac{\beta I_m S_m}{N_m} \\ \frac{dI_m}{dt} = \frac{\beta I_m S_m}{N_m} - \mu I_m \\ \frac{dR_m}{dt} = \mu I_m \end{array} \right.$$

where β is the transmission rate and γ the recovery rate. The dynamics of the various basins are coupled through the travel matrix of the WAN⁹, whose link weights determine the passenger flows among basins. Here we set $\pi_{mn} = w_{mn} / (N_m + N_n)$ as the probability that an individual travels from m to n in a given time step. Simulations start with an initial number of infected $I_0 = 10$ in a designated seed basin and evolve with a transmission rate $\beta = 0.3$ and a recovery rate $\gamma = 0.1$, for 300 time steps.

We select initial seeds as the four most interconnected basins from each continent (Africa, Asia, Europe, North America, South America, and Oceania), resulting in a set of 24 highly connected basins all over the world: Johannesburg, Cairo, Cape

Town, Algiers, Hong Kong, Shanghai, Beijing, Bangkok, London, Paris, Moscow, Milan, New York, Los Angeles, San Francisco, Miami, Sydney, Melbourne, Brisbane, Auckland, Sao Paulo, Rio de Janeiro, Bogota, Santiago. For each seed, we performed 5 simulations on the real network and 20 simulations on different network realizations of the model, for a total of 504 simulations.

Author contributions statement

Designed the analysis: GCi, AV, GCa. Performed the analysis: GF, AM, GCi. Curated the data: JD, AL.

Data and code availability.

Codes that implement the network generation models are available at the github repository <https://github.com/mnlknt/WAN-fitness-modeling>. Raw data are available under commercial license from OAG (www.OAG.org).

References

1. Durlauf, S. N. How can statistical mechanics contribute to social science? *Proc. Natl. Acad. Sci.* **96**, 10582–10584, DOI: [10.1073/pnas.96.19.10582](https://doi.org/10.1073/pnas.96.19.10582) (1999).
2. De Martino, A. & Marsili, M. Statistical mechanics of socio-economic systems with heterogeneous agents. *J. Phys. A: Math. Gen.* **39**, R465, DOI: [10.1088/0305-4470/39/43/R01](https://doi.org/10.1088/0305-4470/39/43/R01) (2006).
3. Castellano, C., Fortunato, S. & Loreto, V. Statistical physics of social dynamics. *Rev. Mod. Phys.* **81**, 591–646, DOI: [10.1103/RevModPhys.81.591](https://doi.org/10.1103/RevModPhys.81.591) (2009).
4. Perc, M. *et al.* Statistical physics of human cooperation. *Phys. Reports* **687**, 1–51, DOI: [10.1016/j.physrep.2017.05.004](https://doi.org/10.1016/j.physrep.2017.05.004) (2017).
5. Caldarelli, G., Wolf, S. & Moreno, Y. Physics of humans, physics for society. *Nat. Phys.* **14**, 870–870, DOI: [10.1038/s41567-018-0266-x](https://doi.org/10.1038/s41567-018-0266-x) (2018).
6. Barthelemy, M. The statistical physics of cities. *Nat. Rev. Phys.* **1**, 406–415, DOI: [10.1038/s42254-019-0054-2](https://doi.org/10.1038/s42254-019-0054-2) (2019).
7. Cimini, G. *et al.* The statistical physics of real-world networks. *Nat. Rev. Phys.* **1**, 58–71, DOI: [10.1038/s42254-018-0002-6](https://doi.org/10.1038/s42254-018-0002-6) (2019).
8. Bouchaud, J.-P. From statistical physics to social sciences: the pitfalls of multi-disciplinarity. *Ind. Corp. Chang.* **34**, 235–248, DOI: [10.1093/icc/dtaf002](https://doi.org/10.1093/icc/dtaf002) (2025).
9. Balcan, D. *et al.* Multiscale mobility networks and the spatial spreading of infectious diseases. *Proc. Natl. Acad. Sci.* **106**, 21484–21489, DOI: [10.1073/pnas.0906910106](https://doi.org/10.1073/pnas.0906910106) (2009).
10. Brockmann, D. & Helbing, D. The hidden geometry of complex, network-driven contagion phenomena. *Science* **342**, 1337–1342, DOI: [10.1126/science.1245200](https://doi.org/10.1126/science.1245200) (2013).
11. Tizzoni, M. *et al.* On the use of human mobility proxies for modeling epidemics. *PLOS Comput. Biol.* **10**, 1–15, DOI: [10.1371/journal.pcbi.1003716](https://doi.org/10.1371/journal.pcbi.1003716) (2014).
12. Pastor-Satorras, R., Castellano, C., Van Mieghem, P. & Vespignani, A. Epidemic processes in complex networks. *Rev. Mod. Phys.* **87**, 925–979, DOI: [10.1103/RevModPhys.87.925](https://doi.org/10.1103/RevModPhys.87.925) (2015).
13. Oliver, N. *et al.* Mobile phone data for informing public health actions across the covid-19 pandemic life cycle. *Sci. Adv.* **6**, eabc0764, DOI: [10.1126/sciadv.abc0764](https://doi.org/10.1126/sciadv.abc0764) (2020).
14. Sills, J. *et al.* Aggregated mobility data could help fight covid-19. *Science* **368**, 145–146, DOI: [10.1126/science.abb8021](https://doi.org/10.1126/science.abb8021) (2020).
15. Wesolowski, A. *et al.* Quantifying the impact of human mobility on malaria. *Science* **338**, 267–270, DOI: [10.1126/science.1223467](https://doi.org/10.1126/science.1223467) (2012).
16. Kostandova, N. *et al.* A systematic review of using population-level human mobility data to understand sars-cov-2 transmission. *Nat. Commun.* **15**, 10504, DOI: [10.1038/s41467-024-54895-7](https://doi.org/10.1038/s41467-024-54895-7) (2024).
17. Lu, X. *et al.* Human mobility in epidemic modeling. *Phys. Reports* **1157**, 1–45, DOI: [10.1016/j.physrep.2025.10.010](https://doi.org/10.1016/j.physrep.2025.10.010) (2026).
18. Flahault, A. & Valleron, A. A method for assessing the global spread of hiv-1 infection based on air travel. *Math. Popul. Stud.* **3**, 161–171, DOI: [10.1080/08898489209525336](https://doi.org/10.1080/08898489209525336) (1992).

19. Grais, R. F., Hugh Ellis, J. & Glass, G. E. Assessing the impact of airline travel on the geographic spread of pandemic influenza. *Eur. J. Epidemiol.* **18**, 1065–1072, DOI: [10.1023/A:1026140019146](https://doi.org/10.1023/A:1026140019146) (2003).
20. Hufnagel, L., Brockmann, D. & Geisel, T. Forecast and control of epidemics in a globalized world. *Proc. Natl. Acad. Sci.* **101**, 15124–15129, DOI: [10.1073/pnas.0308344101](https://doi.org/10.1073/pnas.0308344101) (2004).
21. Colizza, V., Barrat, A., Barthélémy, M. & Vespignani, A. The role of the airline transportation network in the prediction and predictability of global epidemics. *Proc. Natl. Acad. Sci.* **103**, 2015–2020, DOI: [10.1073/pnas.0510525103](https://doi.org/10.1073/pnas.0510525103) (2006).
22. Hollingsworth, T. D., Ferguson, N. M. & Anderson, R. M. Will travel restrictions control the international spread of pandemic influenza? *Nat. Medicine* **12**, 497–499, DOI: [10.1038/nm0506-497](https://doi.org/10.1038/nm0506-497) (2006).
23. Johansson, M. A. *et al.* On the treatment of airline travelers in mathematical models. *PLOS ONE* **6**, 1–7, DOI: [10.1371/journal.pone.0022151](https://doi.org/10.1371/journal.pone.0022151) (2011).
24. Meslé, M. M. I., Hall, I. M., Christley, R. M., Leach, S. & Read, J. M. The use and reporting of airline passenger data for infectious disease modelling: a systematic review. *Eurosurveillance* **24**, 1800216, DOI: [10.2807/1560-7917.ES.2019.24.31.1800216](https://doi.org/10.2807/1560-7917.ES.2019.24.31.1800216) (2019).
25. Davis, J. T. *et al.* Cryptic transmission of sars-cov-2 and the first covid-19 wave. *Nature* **600**, 127–132, DOI: [10.1038/s41586-021-04130-w](https://doi.org/10.1038/s41586-021-04130-w) (2021).
26. Wardle, J., Bhatia, S., Cori, A. & Nouvellet, P. Temporal variations in international air travel: implications for modelling the spread of infectious diseases. *J. Travel. Medicine* **31**, taae062, DOI: [10.1093/jtm/taae062](https://doi.org/10.1093/jtm/taae062) (2024).
27. Lessler, J., Kaufman, J. H., Ford, D. A. & Douglas, J. V. The cost of simplifying air travel when modeling disease spread. *PLOS ONE* **4**, 1–5, DOI: [10.1371/journal.pone.0004403](https://doi.org/10.1371/journal.pone.0004403) (2009).
28. Wardle, J., Bhatia, S., Kraemer, M. U., Nouvellet, P. & Cori, A. Gaps in mobility data and implications for modelling epidemic spread: A scoping review and simulation study. *Epidemics* **42**, 100666, DOI: [10.1016/j.epidem.2023.100666](https://doi.org/10.1016/j.epidem.2023.100666) (2023).
29. National Academies of Sciences Engineering and Medicine. *Improving the CDC Quarantine Station Network's Response to Emerging Threats* (The National Academies Press, Washington, DC, 2022).
30. Grosche, T., Rothlauf, F. & Heinzl, A. Gravity models for airline passenger volume estimation. *J. Air Transp. Manag.* **13**, 175–183, DOI: [10.1016/j.jairtraman.2007.02.001](https://doi.org/10.1016/j.jairtraman.2007.02.001) (2007).
31. Mao, L., Wu, X., Huang, Z. & Tatem, A. J. Modeling monthly flows of global air travel passengers: An open-access data resource. *J. Transp. Geogr.* **48**, 52–60, DOI: [10.1016/j.jtrangeo.2015.08.017](https://doi.org/10.1016/j.jtrangeo.2015.08.017) (2015).
32. Huang, Z., Wu, X., Garcia, A. J., Fik, T. J. & Tatem, A. J. An open-access modeled passenger flow matrix for the global air network in 2010. *PLOS ONE* **8**, 1–9, DOI: [10.1371/journal.pone.0064317](https://doi.org/10.1371/journal.pone.0064317) (2013).
33. Ehsani, S., Sergeeva, E., Murdy, W. & Fox, B. Predicting the skies: A novel model for flight-level passenger traffic forecasting, DOI: <https://arxiv.org/abs/2401.03397> (2024).
34. Barrat, A., Barthélémy, M., Pastor-Satorras, R. & Vespignani, A. The architecture of complex weighted networks. *Proc. Natl. Acad. Sci.* **101**, 3747–3752, DOI: [10.1073/pnas.0400087101](https://doi.org/10.1073/pnas.0400087101) (2004).
35. Zanin, M. & Lillo, F. Modelling the air transport with complex networks: A short review. *The Eur. Phys. J. Special Top.* **215**, 5–21, DOI: [10.1140/epjst/e2013-01711-9](https://doi.org/10.1140/epjst/e2013-01711-9) (2013).
36. Guimerà, R., Mossa, S., Turtschi, A. & Amaral, L. A. N. The worldwide air transportation network: Anomalous centrality, community structure, and cities' global roles. *Proc. Natl. Acad. Sci.* **102**, 7794–7799, DOI: [10.1073/pnas.0407994102](https://doi.org/10.1073/pnas.0407994102) (2005).
37. Diop, I. M., Cherifi, C., Diallo, C. & Cherifi, H. Revealing the component structure of the world air transportation network. *Appl. Netw. Sci.* **6**, 92, DOI: [10.1007/s41109-021-00430-2](https://doi.org/10.1007/s41109-021-00430-2) (2021).
38. Guimerà, R. & Amaral, L. A. N. Modeling the world-wide airport network. *The Eur. Phys. J. B - Condens. Matter* **38**, 381–385, DOI: [10.1140/epjb/e2004-00131-0](https://doi.org/10.1140/epjb/e2004-00131-0) (2004).
39. Bianconi, G. The entropy of randomized network ensembles. *Europhys. Lett.* **81**, 28005, DOI: [10.1209/0295-5075/81/28005](https://doi.org/10.1209/0295-5075/81/28005) (2008).
40. Bianconi, G. *Information theory of spatial network ensembles*, chap. 5 (Edward Elgar Publishing, 2021).
41. Picciolo, F., Squartini, T., Ruzzentini, F., Basosi, R. & Garlaschelli, D. The role of distances in the world trade web. *2012 Eighth Int. Conf. on Signal Image Technol. Internet Based Syst.* 784–792, DOI: [10.1109/SITIS.2012.118](https://doi.org/10.1109/SITIS.2012.118) (2012).

42. Zipf, G. K. The $p_1 p_2/d$ hypothesis: On the intercity movement of persons. *Am. Sociol. Rev.* **11**, 677–686, DOI: [10.2307/2087063](https://doi.org/10.2307/2087063) (1946).

43. Barbosa, H. *et al.* Human mobility: Models and applications. *Phys. Reports* **734**, 1–74, DOI: [10.1016/j.physrep.2018.01.001](https://doi.org/10.1016/j.physrep.2018.01.001) (2018).

44. Simini, F., Barlacchi, G., Luca, M. & Pappalardo, L. A deep gravity model for mobility flows generation. *Nat. Commun.* **12**, 6576, DOI: [10.1038/s41467-021-26752-4](https://doi.org/10.1038/s41467-021-26752-4) (2021).

45. Cabanas-Tirapu, O., Danús, L., Moro, E., Sales-Pardo, M. & Guimerà, R. Human mobility is well described by closed-form gravity-like models learned automatically from data. *Nat. Commun.* **16**, 1336, DOI: [10.1038/s41467-025-56495-5](https://doi.org/10.1038/s41467-025-56495-5) (2025).

46. Anand, K. *et al.* The missing links: A global study on uncovering financial network structures from partial data. *J. Financial Stab.* **35**, 107–119, DOI: [10.1016/j.jfs.2017.05.012](https://doi.org/10.1016/j.jfs.2017.05.012) (2018).

47. Squartini, T., Caldarelli, G., Cimini, G., Gabrielli, A. & Garlaschelli, D. Reconstruction methods for networks: The case of economic and financial systems. *Phys. Reports* **757**, 1–47, DOI: [10.1016/j.physrep.2018.06.008](https://doi.org/10.1016/j.physrep.2018.06.008) (2018).

48. Mistrulli, P. E. Assessing financial contagion in the interbank market: Maximum entropy versus observed interbank lending patterns. *J. Bank. & Finance* **35**, 1114–1127, DOI: [10.1016/j.jbankfin.2010.09.018](https://doi.org/10.1016/j.jbankfin.2010.09.018) (2011).

49. Bardoscia, M. *et al.* The physics of financial networks. *Nat. Rev. Phys.* **3**, 490–507, DOI: [10.1038/s42254-021-00322-5](https://doi.org/10.1038/s42254-021-00322-5) (2021).

50. Caldarelli, G., Capocci, A., Rios, P. D. L. & Muñoz, M. A. Scale-free networks from varying vertex intrinsic fitness. *Phys. Rev. Lett.* **89**, 258702, DOI: [10.1103/PhysRevLett.89.258702](https://doi.org/10.1103/PhysRevLett.89.258702) (2002).

51. Garlaschelli, D. & Loffredo, M. I. Fitness-dependent topological properties of the world trade web. *Phys. Rev. Lett.* **93**, 188701–, DOI: [10.1103/PhysRevLett.93.188701](https://doi.org/10.1103/PhysRevLett.93.188701) (2004).

52. Cimini, G., Squartini, T., Garlaschelli, D. & Gabrielli, A. Systemic risk analysis on reconstructed economic and financial networks. *Sci. Reports* **5**, 15758, DOI: [10.1038/srep15758](https://doi.org/10.1038/srep15758) (2015).

53. Ialongo, L. N. *et al.* Reconstructing firm-level interactions in the dutch input–output network from production constraints. *Sci. Reports* **12**, 11847, DOI: [10.1038/s41598-022-13996-3](https://doi.org/10.1038/s41598-022-13996-3) (2022).

54. Karrer, B. & Newman, M. E. J. Stochastic blockmodels and community structure in networks. *Phys. Rev. E* **83**, 016107, DOI: [10.1103/PhysRevE.83.016107](https://doi.org/10.1103/PhysRevE.83.016107) (2011).

55. Fronczak, P., Fronczak, A. & Bujok, M. Exponential random graph models for networks with community structure. *Phys. Rev. E* **88**, 032810, DOI: [10.1103/PhysRevE.88.032810](https://doi.org/10.1103/PhysRevE.88.032810) (2013).

56. Official aviation guide (oag) worldwide flight and passenger data (2019).

57. Serafino, M. *et al.* True scale-free networks hidden by finite size effects. *Proc. Natl. Acad. Sci.* **118**, e2013825118, DOI: [10.1073/pnas.2013825118](https://doi.org/10.1073/pnas.2013825118) (2021).

58. Newman, M. E. J. Modularity and community structure in networks. *Proc. Natl. Acad. Sci.* **103**, 8577–8582, DOI: [10.1073/pnas.0601602103](https://doi.org/10.1073/pnas.0601602103) (2006).

59. Gabrielli, A., Mastrandrea, R., Caldarelli, G. & Cimini, G. Grand canonical ensemble of weighted networks. *Phys. Rev. E* **99**, 030301, DOI: [10.1103/PhysRevE.99.030301](https://doi.org/10.1103/PhysRevE.99.030301) (2019).

60. Parisi, F., Squartini, T. & Garlaschelli, D. A faster horse on a safer trail: generalized inference for the efficient reconstruction of weighted networks. *New J. Phys.* **22**, 053053, DOI: [10.1088/1367-2630/ab74a7](https://doi.org/10.1088/1367-2630/ab74a7) (2020).

61. Park, J. & Newman, M. E. J. Statistical mechanics of networks. *Phys. Rev. E* **70**, 066117, DOI: [10.1103/PhysRevE.70.066117](https://doi.org/10.1103/PhysRevE.70.066117) (2004).

62. Cover, T. M. & Thomas, J. A. *Elements of Information Theory* (Wiley, 2005).

63. Fronczak, A. *Exponential Random Graph Models*, 810–826 (Springer New York, 2018).

64. Jaynes, E. T. Information theory and statistical mechanics. *Phys. Rev.* **106**, 620–630, DOI: [10.1103/PhysRev.106.620](https://doi.org/10.1103/PhysRev.106.620) (1957).

65. Squartini, T. & Garlaschelli, D. Analytical maximum-likelihood method to detect patterns in real networks. *New J. Phys.* **13**, 083001, DOI: [10.1088/1367-2630/13/8/083001](https://doi.org/10.1088/1367-2630/13/8/083001) (2011).

66. Squartini, T. & Garlaschelli, D. *Maximum-Entropy Networks* (Springer International Publishing, 2017).

67. Vallarano, N. *et al.* Fast and scalable likelihood maximization for exponential random graph models with local constraints. *Sci. Reports* **11**, 15227, DOI: [10.1038/s41598-021-93830-4](https://doi.org/10.1038/s41598-021-93830-4) (2021).

68. Mastrandrea, R., Squartini, T., Fagiolo, G. & Garlaschelli, D. Enhanced reconstruction of weighted networks from strengths and degrees. *New J. Phys.* **16**, 043022, DOI: [10.1088/1367-2630/16/4/043022](https://doi.org/10.1088/1367-2630/16/4/043022) (2014).
69. Cimini, G., Squartini, T., Gabrielli, A. & Garlaschelli, D. Estimating topological properties of weighted networks from limited information. *Phys. Rev. E* **92**, 040802, DOI: [10.1103/PhysRevE.92.040802](https://doi.org/10.1103/PhysRevE.92.040802) (2015).
70. Balcan, D. *et al.* Modeling the spatial spread of infectious diseases: The global epidemic and mobility computational model. *J. Comput. Sci.* **1**, 132–145, DOI: [10.1016/j.jocs.2010.07.002](https://doi.org/10.1016/j.jocs.2010.07.002) (2010).
71. Gonçalves, B. Epidemiology 101. <https://bgoncalves.medium.com/list/epidemiology-101-185b95a0f345>.
72. Bagler, G. Analysis of the airport network of india as a complex weighted network. *Phys. A: Stat. Mech. its Appl.* **387**, 2972–2980, DOI: [10.1016/j.physa.2008.01.077](https://doi.org/10.1016/j.physa.2008.01.077) (2008).
73. Bianconi, G., Pin, P. & Marsili, M. Assessing the relevance of node features for network structure. *Proc. Natl. Acad. Sci.* **106**, 11433–11438, DOI: [10.1073/pnas.0811511106](https://doi.org/10.1073/pnas.0811511106) (2009).

Supplementary Materials

S1 WAN data

The global air-travel data come from the Official Aviation Guide (OAG), which reports the number of passengers flying between airport pairs each month⁵⁶. Specifically these data report the number of people traveling between airport pairs and count each trip only once, from the starting airport to the final destination (ignoring layovers). To generate the basin level network we aggregated data from September to November 2019. We build a seasonal flight network by averaging the passenger flows from these three months. Airports are grouped into larger geographic “basins” which are generated from a Voronoi tessellation centered around major transportation hubs. From this network we can calculate the daily probability of travel between two basin pairs, which is used in the metapopulation model to simulate the global spread of a pathogen. This mobility network has been used previously to study the global spread of infectious diseases⁹.

The Haversine formula

The Haversine formula is used to compute the great-circle distance d between two points on the surface of a sphere given their latitudes and longitudes. In the formula:

$$h = \sin^2\left(\frac{\phi_2 - \phi_1}{2}\right) + \cos(\phi_1) \cos(\phi_2) \sin^2\left(\frac{\lambda_2 - \lambda_1}{2}\right),$$
$$d = 2r \arcsin\left(\sqrt{h}\right),$$

where the variables are defined as follows:

- ϕ_1, ϕ_2 : The latitudes of the first and second points, respectively, measured in radians.
- λ_1, λ_2 : The longitudes of the first and second points, respectively, measured in radians.
- r : The radius of the sphere (for Earth, r is approximately 6,371 km).
- h : An auxiliary value that represents the square of half the chord length between the points. It is computed using the differences in latitudes and longitudes.
- d : The great-circle distance between the two points along the surface of the sphere.

S2 Model formulations

Here we describe different model formulations we tested for reconstructing the WAN, for the general case of weighted directed networks. Each link $i \rightarrow j$ has weight $w_{i \rightarrow j}$ (in general $\neq w_{j \rightarrow i}$), hence each node i is characterized by a value of in-strength $s_i^{\text{in}} = \sum_j w_{j \rightarrow i}$ and out-strength $s_i^{\text{out}} = \sum_j w_{i \rightarrow j}$. If the network is undirected (meaning $w_{i \rightarrow j} = w_{j \rightarrow i} \equiv w_{ij}$), there is only one strength value per node, hence it is enough to replace $s_i^{\text{out}} = s_i^{\text{in}}$ with $s_i = \sum_j w_{ij}$ (for models **B** and **C**, this holds also for block-specific strengths).

Model K. The fitness-induced, density-corrected Gravity Model, proposed in⁵² to reconstruct economic and financial networks, is based on two inference steps. First, links are drawn according to the canonical *configuration model* (CM) prescription, relying on a fitness assumption that nodes with large passenger flux are likely to be connected. Hence the (CM) parameters controlling degrees are replaced with node strengths. Thus, each link $i \rightarrow j$ (with $i \neq j$) is sampled independently according to the connection probability

$$p_{i \rightarrow j}^{(\mathbf{K})} = \frac{z^{(\mathbf{K})} s_i^{\text{out}} s_j^{\text{in}}}{1 + z^{(\mathbf{K})} s_i^{\text{out}} s_j^{\text{in}}} \quad (1)$$

which depends on s_i^{out} and s_j^{in} (the required inputs of the model). The only free parameter, $z^{(\mathbf{K})}$, is determined by setting the expected number of links of the network to the empirical value: $L_{\text{tot}} = \sum_i \sum_{j(\neq i)} p_{i \rightarrow j}^{(\mathbf{K})}$ (see Table S2). Second, every sampled link $i \rightarrow j$ (realized with probability $p_{i \rightarrow j}^{(\mathbf{K})}$) is assigned weight

$$w_{i \rightarrow j}^{(\mathbf{K})} = \frac{s_i^{\text{out}} s_j^{\text{in}}}{W \cdot p_{i \rightarrow j}^{(\mathbf{K})}} \quad (2)$$

where $W = \sum_i s_i^{\text{out}} = \sum_i s_i^{\text{in}}$ is the total weight of the network, and $w_{i \rightarrow j}^{(\mathbf{K})} = 0$ otherwise. The model thus generates sparse topologies but, at the same time, the average link weight reads $\langle w_{i \rightarrow j}^{(\mathbf{K})} \rangle = s_i^{\text{out}} s_j^{\text{in}} / W$, analogously to what prescribed by standard maximum-entropy gravity models^{47,48}. Therefore the model preserves, as ensemble averages, the in- and out- strength of each node: $\langle s_i^{\text{out}} \rangle = \sum_j \langle w_{i \rightarrow j}^{(\mathbf{K})} \rangle \equiv s_i^{\text{out}}$ and $\langle s_i^{\text{in}} \rangle = \sum_j \langle w_{j \rightarrow i}^{(\mathbf{K})} \rangle \equiv s_i^{\text{in}}$.

Model S. For sparse networks, the fitness ansatz of model **K** actually means assuming that degrees are linearly proportional to strengths. However for the WAN it is known that $s(k) \sim k^\beta$ with $\beta > 1$ ^{34,38,72}. We can thus employ a non-linear fitness ansatz of this form, leading to model formulation **S** where the connection probability takes the form:

$$p_{i \rightarrow j}^{(\mathbf{S})} = \frac{z^{(\mathbf{S})} [s_i^{\text{out}} s_j^{\text{in}}]^\alpha}{1 + z^{(\mathbf{S})} [s_i^{\text{out}} s_j^{\text{in}}]^\alpha}. \quad (3)$$

and the parameter $z^{(\mathbf{S})}$ is obtained as before (see Table S2). We set the optimal exponent α by minimizing the RMSD between the empirical and reconstructed degree sequences (see Figure S5). For weights we keep the same functional form of eq. (2): $w_{i \rightarrow j}^{(\mathbf{S})} = s_i^{\text{out}} s_j^{\text{in}} / (W \cdot p_{i \rightarrow j}^{(\mathbf{S})})$ with probability $p_{i \rightarrow j}^{(\mathbf{S})}$ and $w_{i \rightarrow j}^{(\mathbf{S})} = 0$ otherwise, hence also model **S** preserves, as ensemble averages, the in- and out- strength of each node. In the regime of very sparse networks, where $p_{i \rightarrow j}^{(\mathbf{S})} \sim z^{(\mathbf{S})} [s_i^{\text{out}} s_j^{\text{in}}]^\alpha$, this leads to $w_{i \rightarrow j}^{(\mathbf{S})} \sim (k_i^{\text{out}} k_j^{\text{in}})^\beta (1 - \alpha)$, with values of the exponent compatible with empirical findings of³⁴.

Model D. In order to introduce a dependency on the distance between airports, we follow the maximum entropy construction for spatial networks^{39,40,73}, prescribing to constrain the node degrees and the number of links at a certain distance interval. Merging this recipe with the fitness ansatz leads to model formulation **D**:

$$p_{i \rightarrow j}^{(\mathbf{D})} = \frac{z^{(\mathbf{D})} s_i^{\text{out}} s_j^{\text{in}} l(d_{ij})}{1 + z^{(\mathbf{D})} s_i^{\text{out}} s_j^{\text{in}} l(d_{ij})} \quad (4)$$

where d_{ij} is the distance between nodes i and j , $l(d)$ is the probability of having a link between nodes at distance d , and $z^{(\mathbf{D})}$ is obtained as before (see Table S2). Note that the function $l(d)$ is related to the cost of establishing a link between nodes at distance d ; if $l(d)$ is exponential then the cost is linear in d , while a power-law $l(d)$ means that the cost is logarithmic in d ⁴⁰. Weights are again assigned as for eq. (2): $w_{i \rightarrow j}^{(\mathbf{D})} = s_i^{\text{out}} s_j^{\text{in}} / (W \cdot p_{i \rightarrow j}^{(\mathbf{D})})$ with probability $p_{i \rightarrow j}^{(\mathbf{D})}$ and $w_{i \rightarrow j}^{(\mathbf{D})} = 0$ otherwise. Note that model **D** weights do depend on the distance through the connection probabilities, while still preserving on average the in- and out- strength of each node.

Model B (used in the main text). In order to impose a community structure on the model network while keeping the degree constraints, we employ a composition of models **K** – one for each block. We thus split the network nodes into a set of communities $\{g\}$; then we endow each node i with $|g|$ block-specific values of in- and out-strength, $s_{g \rightarrow i}^{\text{in}} = \sum_{j(\neq i) \in g} w_{j \rightarrow i}$ and $s_{i \rightarrow g}^{\text{out}} = \sum_{j(\neq i) \in g} w_{i \rightarrow j}$, each quantifying the connectivity of i with respect to nodes in community g . The probability of connection from node i to node j , belonging respectively to community g_i and g_j , thus reads:

$$p_{i \rightarrow j}^{(\mathbf{B})} = \frac{z_{g_i g_j}^{(\mathbf{B})} s_{i \rightarrow g_j}^{\text{out}} s_{g_i \rightarrow j}^{\text{in}}}{1 + z_{g_i g_j}^{(\mathbf{B})} s_{i \rightarrow g_j}^{\text{out}} s_{g_i \rightarrow j}^{\text{in}}} \quad (5)$$

where the parameters $z_{g_i g_j}^{(\mathbf{B})}$ can be computed through the set of equations $\sum_{i \in g_i} \sum_{j \in g_j} p_{i \rightarrow j}^{(\mathbf{B})} = L_{g_i, g_j}$ (see Figure S4). Weights are then assigned as $w_{i \rightarrow j}^{(\mathbf{B})} = s_{i \rightarrow g_j}^{\text{out}} s_{g_i \rightarrow j}^{\text{in}} / (W_{g_i g_j} \cdot p_{i \rightarrow j}^{(\mathbf{B})})$ with probability $p_{i \rightarrow j}^{(\mathbf{B})}$ and $w_{i \rightarrow j}^{(\mathbf{B})} = 0$ otherwise, where now $W_{g_i g_j} = \sum_{i \in g_i} \sum_{j \in g_j} w_{i \rightarrow j}$ is the total weight of connections from nodes in g_i to nodes in g_j . Therefore the model preserves, as ensemble averages, the out-strength and the in-strength by group of each node: $\langle s_{g_i \rightarrow j}^{\text{in}} \rangle = \sum_{i \in g_i} \langle w_{i \rightarrow j}^{(\mathbf{B})} \rangle \equiv s_{g_i \rightarrow j}^{\text{in}}$ and $\langle s_{i \rightarrow g_j}^{\text{out}} \rangle = \sum_{j \in g_j} \langle w_{i \rightarrow j}^{(\mathbf{B})} \rangle \equiv s_{i \rightarrow g_j}^{\text{out}}$.

Model C. The combined model that incorporates all ingredients of the previous formulations is based on the same community structure $\{g\}$ of model **B**, so that the probability of connection from node i to node j , belonging respectively to community g_i and g_j , is:

$$p_{i \rightarrow j}^{(\mathbf{C})} = \frac{z_{g_i g_j}^{(\mathbf{C})} [s_{i \rightarrow g_j}^{\text{out}} s_{g_i \rightarrow j}^{\text{in}}]^{\alpha} l(d_{ij})}{1 + z_{g_i g_j}^{(\mathbf{C})} [s_{i \rightarrow g_j}^{\text{out}} s_{g_i \rightarrow j}^{\text{in}}]^{\alpha} l(d_{ij})} \quad (6)$$

where $l(d_{ij})$ is the geographic distance between nodes i and j , while the optimal exponent α is set to minimize the RMSD between the empirical and reconstructed degree sequences (see Figure S5). The parameters $z_{g_i g_j}^{(\mathbf{C})}$ can be computed through the set of equations $\sum_{i \in g_i} \sum_{j \in g_j} p_{i \rightarrow j}^{(\mathbf{C})} = L_{g_i, g_j}$ (see Figure S4). Weights are then assigned as $w_{i \rightarrow j}^{(\mathbf{C})} = s_{i \rightarrow g_j}^{\text{out}} s_{g_i \rightarrow j}^{\text{in}} / (W_{g_i g_j} \cdot p_{i \rightarrow j}^{(\mathbf{C})})$ with probability $p_{i \rightarrow j}^{(\mathbf{C})}$ and $w_{i \rightarrow j}^{(\mathbf{C})} = 0$ otherwise. Thus model **C** preserves, as ensemble averages, the out-strength and the in-strength by group of each node – as model **B** does.

Model R. As benchmark we consider model **R** of a random network with the same density of WAN, hence $p_{i \rightarrow j}^{(\mathbf{R})} \equiv \bar{p} = L_{\text{tot}} / [N(N-1)] \forall i, j$. This results in $k_i^{(\mathbf{R})} = L_{\text{tot}} / N \forall i$. For weights, $w_{i \rightarrow j}^{(\mathbf{R})} = s_i^{\text{out}} s_j^{\text{in}} / (W \bar{p})$ with probability \bar{p} .

Model	Equation	z (basin)	residual error	z (airport)	residual error
K	$\sum_{ij} a_{i \rightarrow j} = \sum_i \sum_{j(\neq i)} \frac{z^{(K)} s_i^{\text{out}} s_j^{\text{in}}}{1 + z^{(K)} s_i^{\text{out}} s_j^{\text{in}}}$	$5.70 \cdot 10^{-9}$	$-1 \cdot 10^{-12}$	$2.44 \cdot 10^{-11}$	$-5 \cdot 10^{-11}$
S	$\sum_{ij} a_{i \rightarrow j} = \sum_i \sum_{j(\neq i)} \frac{z^{(S)} [s_i^{\text{out}} s_j^{\text{in}}]^\alpha}{1 + z^{(S)} [s_i^{\text{out}} s_j^{\text{in}}]^\alpha}$	$1.69 \cdot 10^{-7}$	$-1 \cdot 10^{-11}$	$1.33 \cdot 10^{-8}$	$2 \cdot 10^{-11}$
D	$\sum_{ij} a_{i \rightarrow j} = \sum_i \sum_{j(\neq i)} \frac{z^{(D)} s_i^{\text{out}} s_j^{\text{in}} l(d_{ij})}{1 + z^{(D)} s_i^{\text{out}} s_j^{\text{in}} l(d_{ij})}$	$8.58 \cdot 10^{-7}$	$5 \cdot 10^{-12}$	$1.57 \cdot 10^{-9}$	$2 \cdot 10^{-11}$

Table S2. For models **K**, **S** and **D**, the parameter z is determined by equating the total number of links of the model network, namely $\sum_i \sum_{j(\neq i)} p_{i \rightarrow j}$, with the number of links of the real network $L_{\text{tot}} = \sum_i \sum_{j(\neq i)} a_{i \rightarrow j}$. Here we report the specific equation for each model and the corresponding value of z .

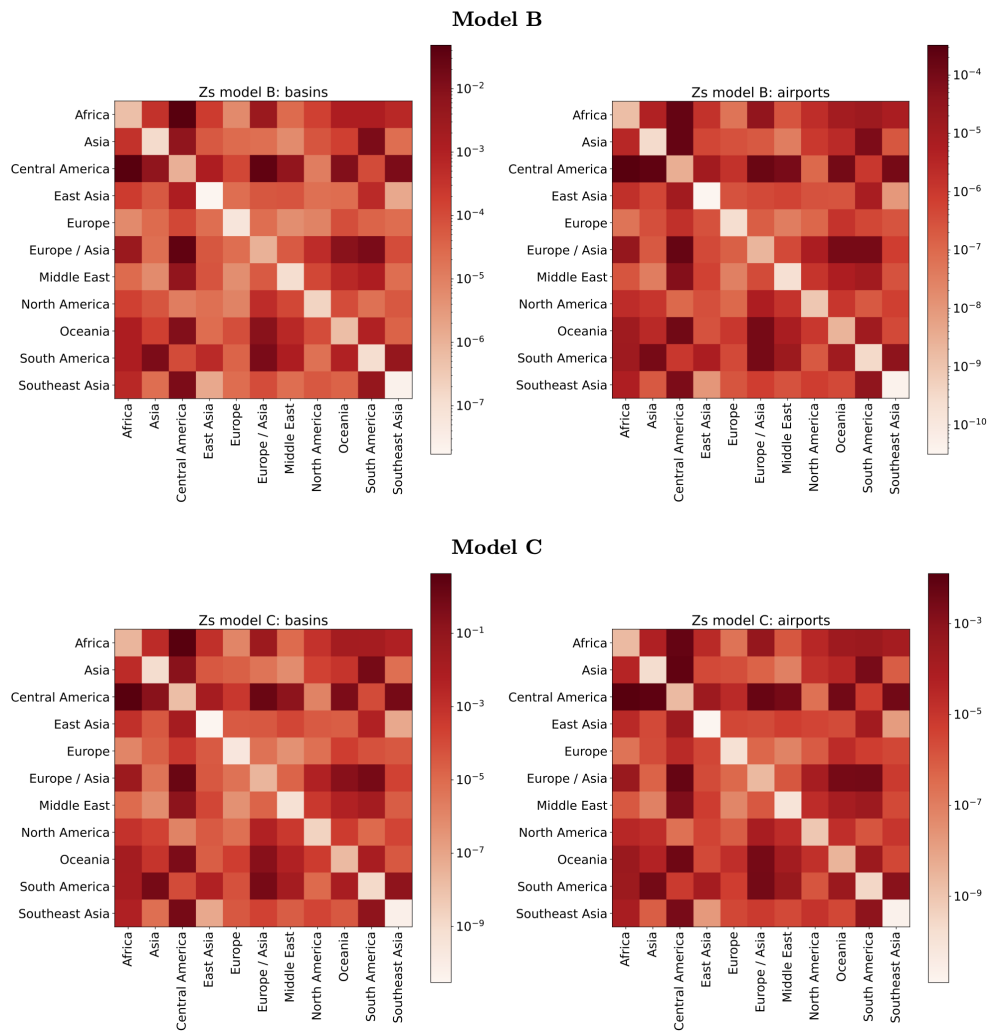


Figure S4. For models **B** and **C**, the parameter $z_{g_i g_j}$ for each pair of communities (g_i, g_j) is determined by equating the total number of links of the model network, namely $\sum_{i \in g_i} \sum_{j(\neq i) \in g_j} p_{i \rightarrow j}$, with the number of links of the real network $L_{g_i g_j} = i \in g_i \sum_{j(\neq i) \in g_j} a_{i \rightarrow j}$. Here we report the specific equation for each model and the heat maps with the corresponding values of z for each pair of regions.

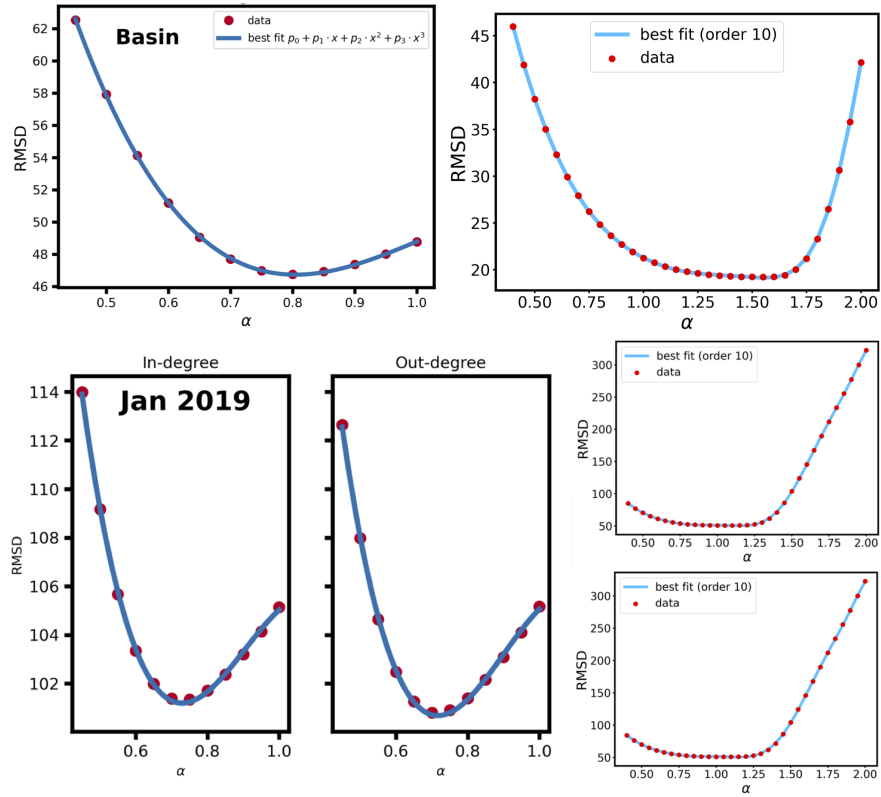


Figure S5. We obtain the optimal α exponent for models **S** and **C** by minimizing the RMSD between the real and reconstructed degree sequence as a function of α . Basins dataset (upper plots): for **S** (left plot) we fitted the curve with a 3rd degree polynomial, yielding the minimum value $\alpha = 0.80$; for **C** (right plot) we used a 10th degree polynomial, yielding $\alpha = 1.56$. Airport dataset (lower plots): for **S** (left plot), $\alpha = 0.72$; for **C** (right plot), $\alpha = 1.16$.

S3 Results for the different model formulations (basins dataset)

Here we discuss and compare the results of all model formulations in reconstructing the topological and dynamical features of the WAN (see Tables S3 and S4 for an overview of the results and the following plots for more detailed comparison). Firstly, by construction all models can reproduce the strength sequence. Concerning the reconstruction of degree values (a baseline requirement, supporting the validity of the ansatz), all models perform fairly well, except of course model **R** that generates a network with constant average degree and achieves a very low recall of 0.018 (i.e., the value of the network density).

With respect to the benchmark model **R**, the simple model **K** brings a very large improvement on recall as well as on the agreement between model and empirical link probabilities. Furthermore, it can well interpolate the degree vs strength relation but is not able to capture its dispersion. However, it fails in reproducing both the dependence of link occurrence on distance and the community structure of the network. Concerning epidemic simulations, **K** generally improves with respect to the random benchmark **R**, but tends to anticipate the epidemic peak and leads to a more homogeneously diffused prevalence map than simulations on the real network.

Model **S**, incorporating the super-linear relation between strengths and degrees, improves on **K** in reconstructing degrees and connection probabilities, but leads to worse recall and reconstruction of topological features: it slightly improves in the interpolation of the relation k vs s but is not able to capture its dispersion; moreover it fails in reproducing both the dependence on distance and the community structure of the network. Model **D**, designed to capture the dependence of connection probabilities on geographical distances, shows a rather opposite behavior. With respect to **K**, the reconstruction of connection probabilities and degrees does not improve while recall increases a lot. Notably, **D** also captures some of the dispersion of the k vs s relation, but not the community structure of the network and, importantly, is not able to improve in reproducing the dependence of link probability on distance. This suggests that air travel is not much affected by the underlying metric space, but rather depends on the geographic area of origin and destination (constrained by model **B**). Concerning epidemic simulations, both models **S** and **D** slightly improve on model **K**, but outcomes remain rather distinct from those simulated on the empirical network.

As discussed in the main text, model **B** improves in any aspect with respect to all other models. Interestingly, the full model **C** (incorporating, at the same time, the ingredients of **S**, **D**, **B**) does not perform as well as model **B**. This suggests that the presence of multiple determinants for links presence is adding noise, rather than improving the signal.

Models	RMSRE _s	RMSRE _k	RMSRE _p	RMSRE _w	Recall	β	MSE _{l(d)}	M
K	10^{-3}	0.34	0.03	0.17	0.31	1.10(5)	9.55	0.0
S	10^{-3}	0.18	0.004	0.17	0.26	1.35(4)	17.6	0.0
D	10^{-3}	0.32	0.02	0.17	0.40	1.07(3)	9.80	0.0
B	10^{-2}	0.18	0.016	0.063	0.75	1.17(0)	2.21	0.63
C	10^{-2}	0.26	0.022	0.089	0.64	0.91(2)	1.04	0.63
R	10^{-3}	10	0.98	0.073	0.018	(4)	162	0.0
Data	-	-	-	-	-	1.2(2)	-	0.67

Table S3. Reconstruction of network properties. (Left sector) Values of Root Mean Squared Relative Error $\sqrt{n^{-1} \sum_i (\langle y_i \rangle / y_i - 1)^2}$ of reconstructed quantities $\langle y_i \rangle$ against empirical observations y_i : RMSRE_s of model strengths $\langle s_i \rangle = \sum_{j \neq i} \langle w \rangle_{ij}$ versus empirical strengths $s_i = \sum_{j \neq i} w_{ij}$; RMSRE_k of model degrees $\langle k_i \rangle = \sum_{j \neq i} p_{ij}$ versus empirical degrees $k_i = \sum_{j \neq i} a_{ij}$; RMSRE_p of empirical link probability f_{ij} versus model link probability p_{ij} ; RMSRE_w of average model weights $\langle w \rangle_{ij}$ versus empirical weights w_{ij} . Recall values for link prediction, obtained using the model link probability to determine the outcome of a binary classification test on the existence of a link. (Left sector) OLS fit exponent β of the strengths vs degrees relation (uncertainties are given in parentheses and refer to the last significant digit); Mean Squared Error (MSE) between empirical and model curve of link probability as a function of distance; average modularity M of the network. “Data” values are those computed on the real network.

Model	Δ area	L2[i]	Peak time	Peak magn.	Epid. length	RMSE[i _m]	L2[H]
K	2.2 ± 0.8	0.29 ± 0.10	9.2 ± 4.4	0.016 ± 0.009	14.6 ± 4.6	0.060 ± 0.007	20 ± 5
S	2.0 ± 0.8	0.27 ± 0.11	8.3 ± 4.2	0.016 ± 0.008	11.0 ± 5.0	0.058 ± 0.008	17 ± 5
D	2.0 ± 0.8	0.27 ± 0.10	8.1 ± 4.0	0.015 ± 0.010	9.5 ± 4.7	0.064 ± 0.009	17 ± 5
B	0.56 ± 0.31	0.073 ± 0.040	2.3 ± 1.8	0.0048 ± 0.0035	4.5 ± 3.2	0.050 ± 0.006	14 ± 6
C	0.61 ± 0.34	0.080 ± 0.043	2.3 ± 1.8	0.0050 ± 0.0038	7.0 ± 3.0	0.063 ± 0.010	18 ± 7
R	2.4 ± 1.1	0.31 ± 0.13	8.6 ± 5.2	0.012 ± 0.008	8.5 ± 6.3	0.079 ± 0.019	22 ± 8
Data	0.43 ± 0.32	0.058 ± 0.042	2.0 ± 1.7	0.0043 ± 0.0034	2.2 ± 2.2	0.024 ± 0.005	13 ± 6

Table S4. Similarity of epidemic simulations on real and model networks. Given a pair of simulations, respectively on the *real* network and a *model* instance, we compute: the area between the prevalence curves, $\Delta = \sum_t |i(t)_{\text{real}} - i(t)_{\text{model}}|$; their L2 distance $\text{L2}[i] = \sqrt{\sum_t [i(t)_{\text{real}} - i(t)_{\text{model}}]^2}$; the peak time difference $\Delta t^* = |t^*_{\text{real}} - t^*_{\text{model}}|$, where $t^*_{\text{real}} = \arg \max_t i(t)_{\text{real}}$ and similarly for t^*_{model} ; the peak magnitude difference $\Delta i^* = |i^*_{\text{real}} - i^*_{\text{model}}|$, with $i^*_{\text{real}} = \max_t i(t)_{\text{real}}$ and similarly for i^*_{model} ; the difference in epidemic lengths $\Delta L = |L_{\text{real}} - L_{\text{model}}|$, where $L_{\text{real}} = (t^{\text{end}})_{\text{real}} - (t^{\text{start}})_{\text{real}}$ and $(t^{\text{start}})_{\text{real}}$ and $(t^{\text{end}})_{\text{real}}$ denote the first and last times at which $i(t)_{\text{real}}$ exceeds a small threshold ε (and analogously for L_{model}); RMSE of prevalence vector averaged over time, $\text{RMSE}[i_m] = T^{-1} \sum_t \sqrt{N^{-1} \sum_m [(i_m(t))_{\text{real}} - (i_m(t))_{\text{model}}]^2}$; normalized L2 distance of the entropy curves, $\text{L2}[H] = \sqrt{\sum_t [H(t)_{\text{real}} - H(t)_{\text{model}}]^2}$. Values in each row are averages over pairwise comparisons of a simulation on the empirical network (x5) and on a network generated by the corresponding model (x20), for each of the 24 seed basins. “Data” values instead are averages over pairwise comparisons of simulations on the empirical network (x5), for each of the 24 seed basins. Uncertainties are given as standard deviations of pairwise comparisons.

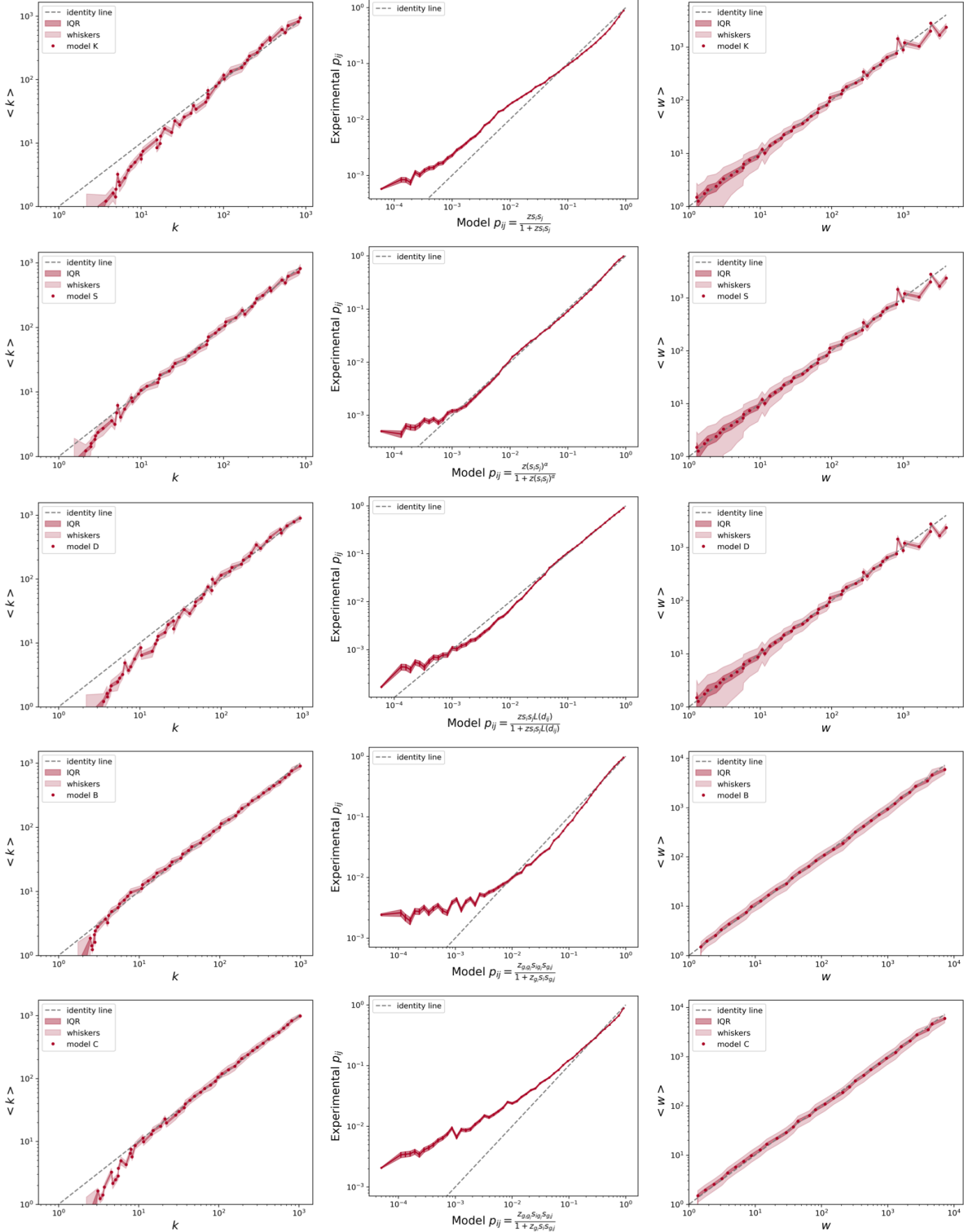


Figure S6. Reconstruction of binary and weighted properties of the WAN. From top to bottom: Models **K**, **S**, **D**, **B**, **C** (Model **R** is not shown). The dashed identity line marks the perfect agreement between empirical and model values. The shaded regions represent the interquartile range and the whiskers of the set of model values. Left column: Model degrees versus observed degrees. Central column: Observed link probability as a function of model link probability. Right column: Model versus observed weights.

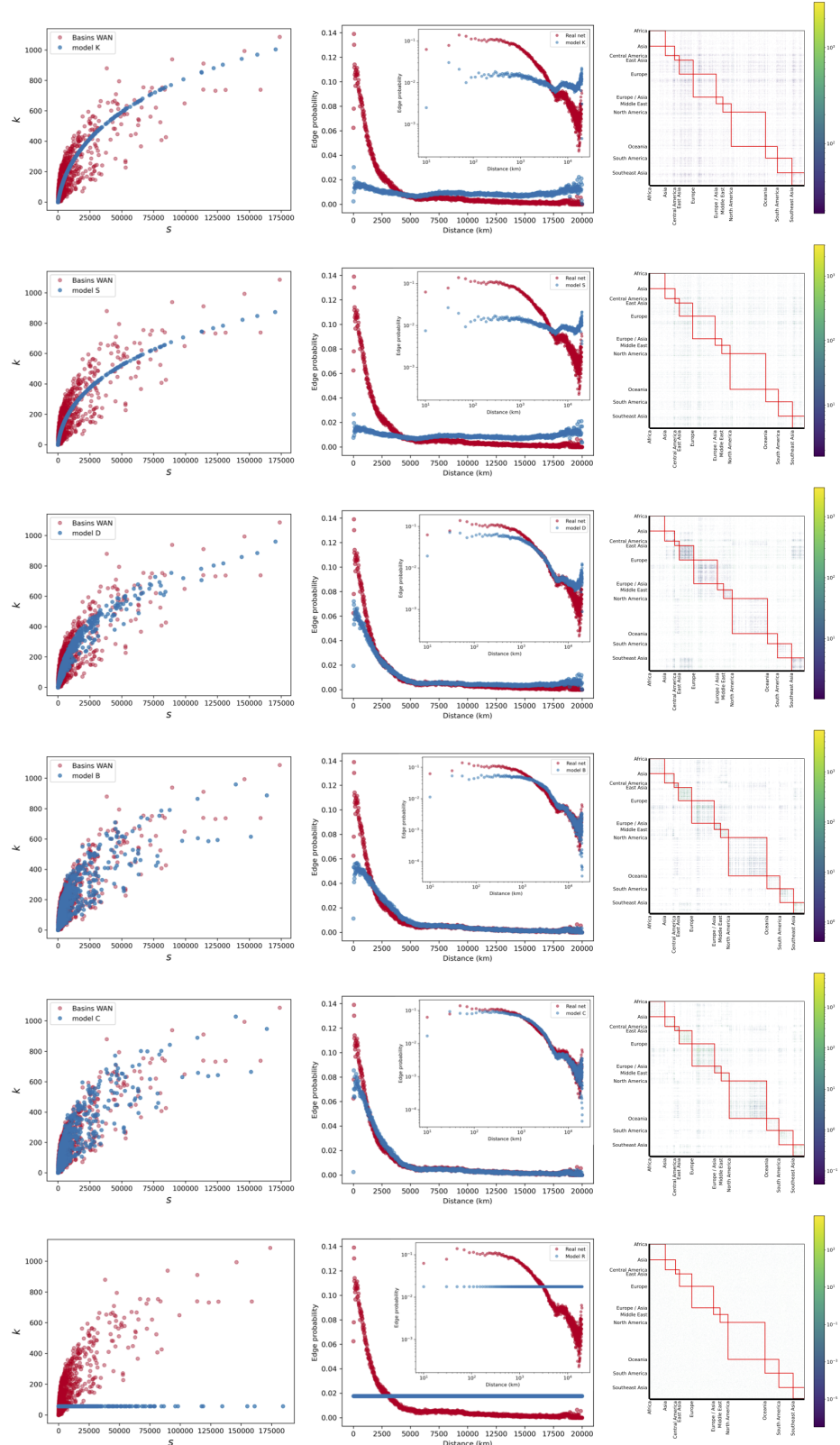


Figure S7. Properties of the reconstructed networks. From top to bottom: Models **K**, **S**, **D**, **B**, **C** (Model **R** is not shown). Left column: degrees vs strengths. Central column: link probability as a function of distance. Right column: community structure.

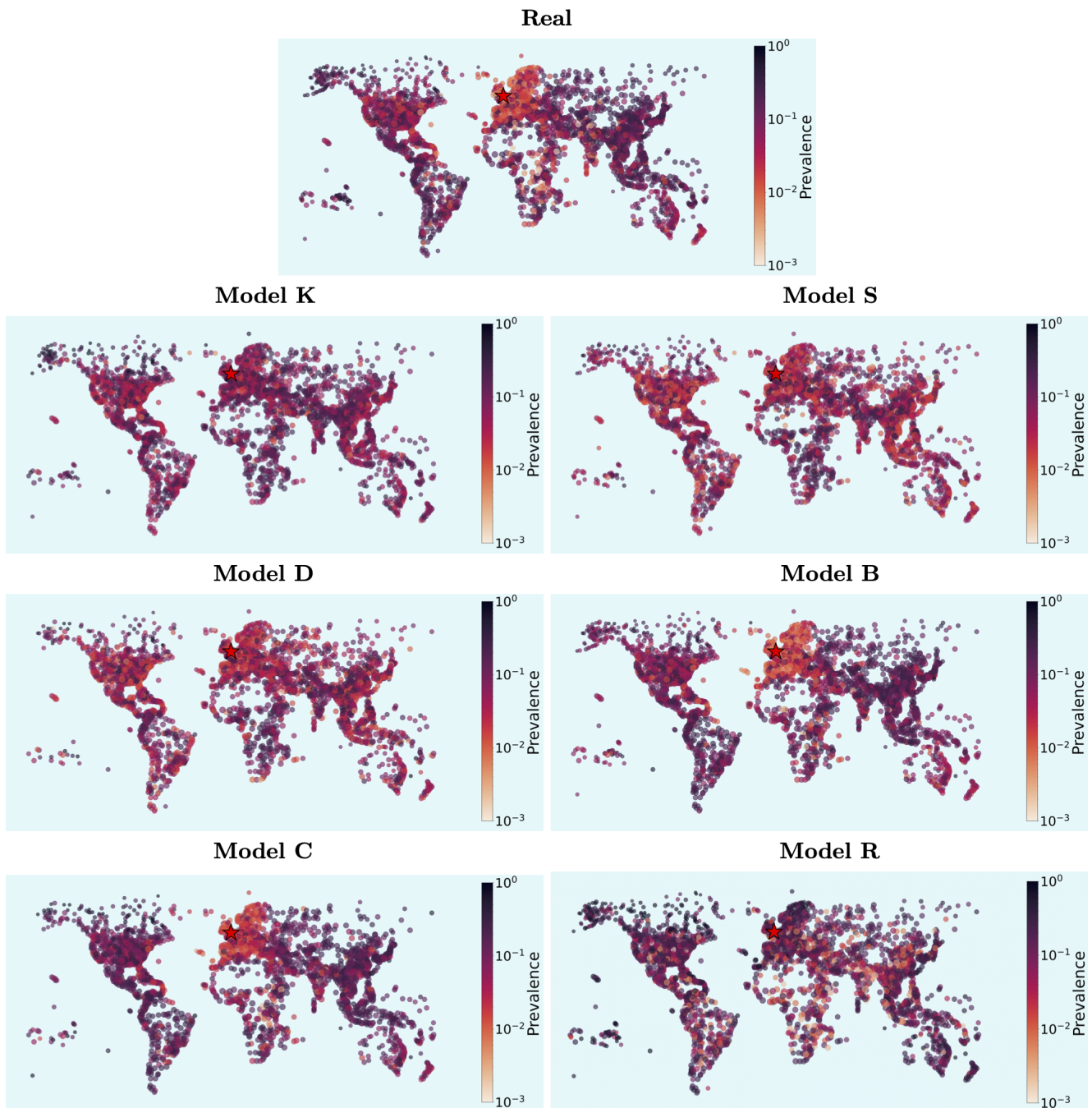
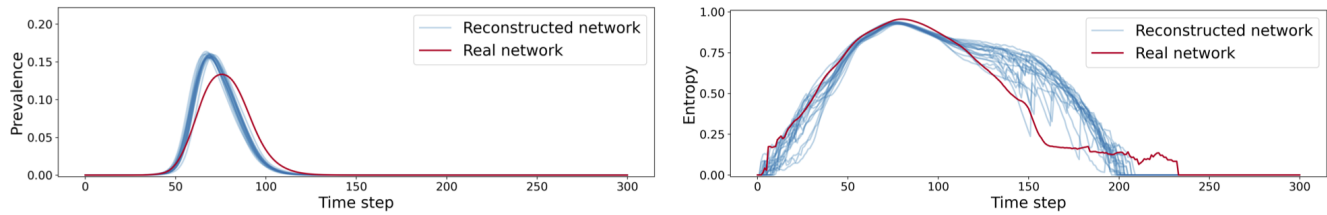
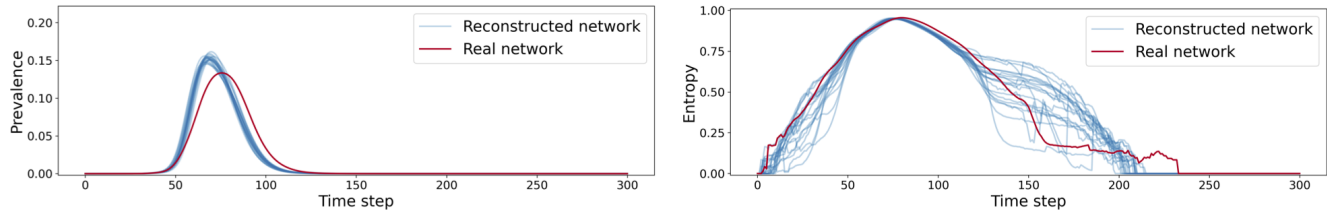


Figure S8. Prevalence maps for the real and model WAN, concerning simulations with seed=London, at time step $t = 80$.

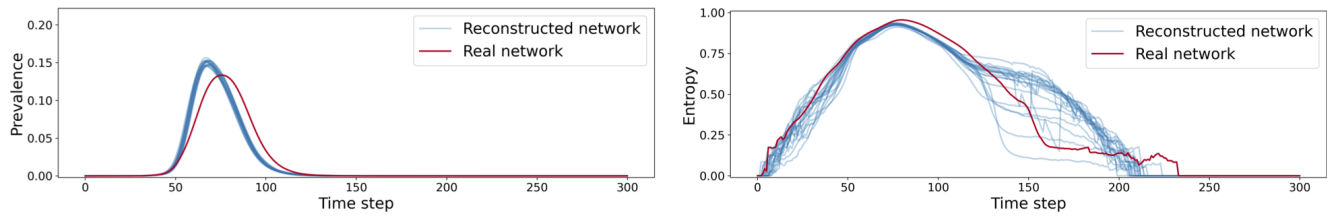
Model K



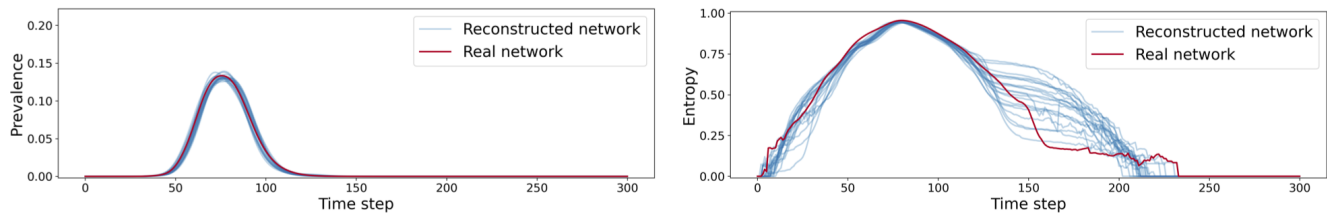
Model S



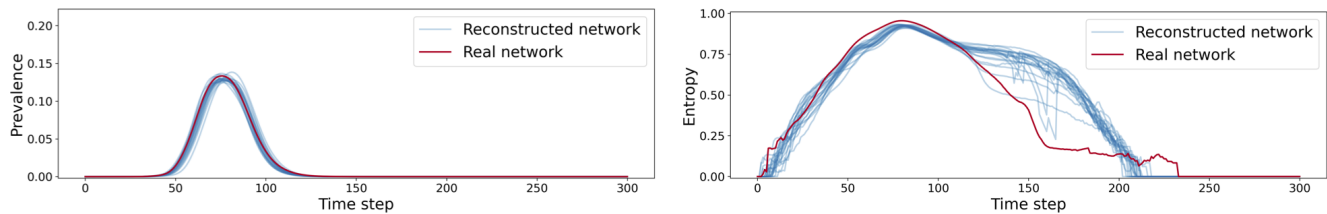
Model D



Model B



Model C



Model R

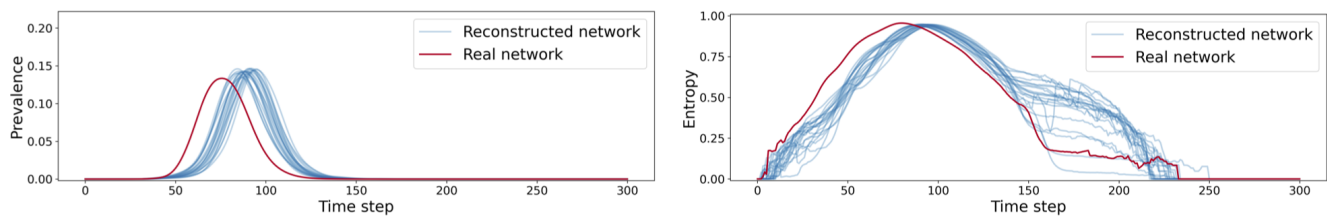


Figure S9. Metapopulation results for seed = London. Comparison of one real simulation and 20 model simulations, in terms of the time evolution of total prevalence and entropy of the prevalence distribution.

S4 Results for the airport-based WAN

We also consider the WAN representation where nodes correspond to individual airports and links denote the flow of passengers between airports. The network is directed in this case, meaning that the weight of the link $w_{i \rightarrow j}$ is the number of passengers traveling from airport i to airport j per month. Here we consider passengers traveling in January of 2019 and airports that send out at least 100 travelers per month. The in and out strength of node i , given by $s_i^{\text{in}} = \sum_j w_{j \rightarrow i}$ and $s_i^{\text{out}} = \sum_j w_{i \rightarrow j}$, represent the number of incoming and outgoing passengers at the corresponding airport, whereas, the in degree $k_i^{\text{in}} = \sum_j a_{j \rightarrow i}$ and out degree $k_i^{\text{out}} = \sum_j a_{i \rightarrow j}$ are the number of direct connections from and to other airports ($a_{i \rightarrow j} = 1$ if $w_{i \rightarrow j} > 0$ and zero otherwise). Note that most of the links are reciprocal³⁵ (the link reciprocity coefficient is 0.9999 and the correlation between the weights of opposed links is 0.9978). The geographic distance between airports i and j is obtained using the Haversine formula, while the geographic communities are defined as for the basin dataset. Analyses on this dataset (reported below) confirm the findings obtained for the basin representation of the WAN concerning the topological reconstruction of the network.

Model	RMSRE $_{s_{in}}$	RMSRE $_{s_{out}}$	RMSRE $_{k_{in}}$	RMSRE $_{k_{out}}$	RMSRE $_{p}$	RMSRE $_{w}$
K	10^{-3}	10^{-3}	0.40	0.40	0.0043	0.15
S	10^{-3}	10^{-3}	0.40	0.18	0.0054	0.15
D	10^{-3}	10^{-3}	0.39	0.39	0.0028	0.15
B	10^{-2}	10^{-2}	0.16	0.18	0.0015	0.15
C	10^{-2}	10^{-2}	0.39	0.36	0.0018	0.13
R	10^{-3}	10^{-3}	7.3	7.4	0.98	0.14

Model	Recall	β_{in}	β_{out}	MSE $_{l(d)}$	M
K	0.36	1.39(5)	1.39(7)	51.1	0.0
S	0.30	1.78(7)	1.78(8)	87.2	0.0
D	0.41	1.37(4)	1.37(5)	45.0	0.0
B	0.73	1.0(8)	1.0(8)	4.25	0.63
C	0.61	1.0(0)	1.0(0)	3.22	0.63
R	0.019	(0)	(4)	200	0.0

Table S5. Reconstruction of network properties for the airport dataset. Values of Root Mean Squared Relative Error $\sqrt{n^{-1} \sum_i (\langle y_i \rangle / y_i - 1)^2}$ of reconstructed quantities $\langle y_i \rangle$ against empirical observations y_i : RMSRE $_s$ of model versus empirical in/out-strengths; RMSRE $_k$ of model versus empirical in/out-degrees; RMSRE $_p$ of empirical link probability versus model link probability; RMSRE $_w$ of model versus empirical weights. Recall values for link prediction, obtained using the model link probability to determine the outcome of a binary classification test on the existence of a link. OLS fit exponent β of the strengths vs degrees relation; Mean Squared Error (MSE) between empirical and model curve of link probability as a function of distance; average modularity M of the network. For real data: $\beta_{in} = 0.9(1)$, $\beta_{out} = 0.9(2)$, $M = 0.64$

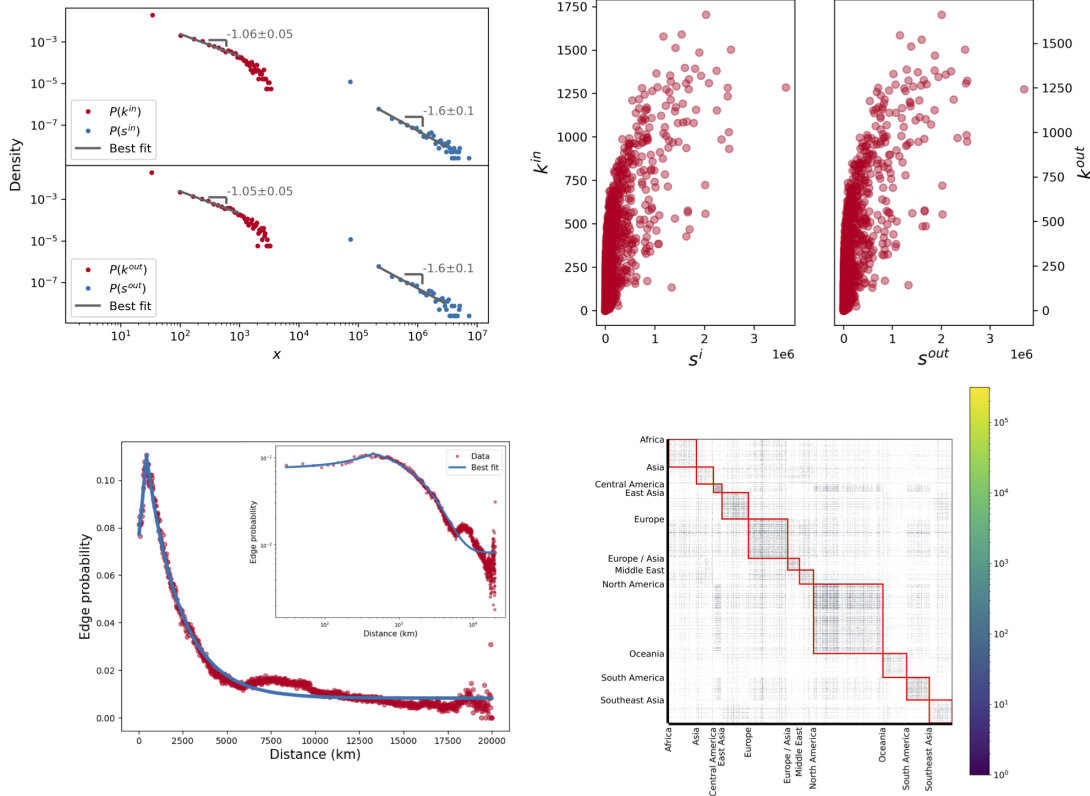


Figure S10. Topological features of the WAN (airport dataset). (A) In/Out-Degree and In/Out-Strength distributions. (B) In/Out-Degrees as a function of In/Out-Strengths, with OLS fit exponents $\beta_{in} = 0.9(1)$ and $\beta_{out} = 0.9(2)$. (C) Link probability as a function of distance. Best fit parameters for the linear part: $d^* = 450\text{km}$, $m = 5.(9) \cdot 10^{-5}$ and $q = 7.(9) \cdot 10^{-2}$ ($R^2 = 0.83$); for the exponential decay: $d_0 = -38.(8) \cdot 10^2$, $a = 52.(5) \cdot 10^{-5}$, $b = 8.(2) \cdot 10^{-3}$ ($R^2 = 0.98$). (D) Block structure, with modularity $M = 0.64$.

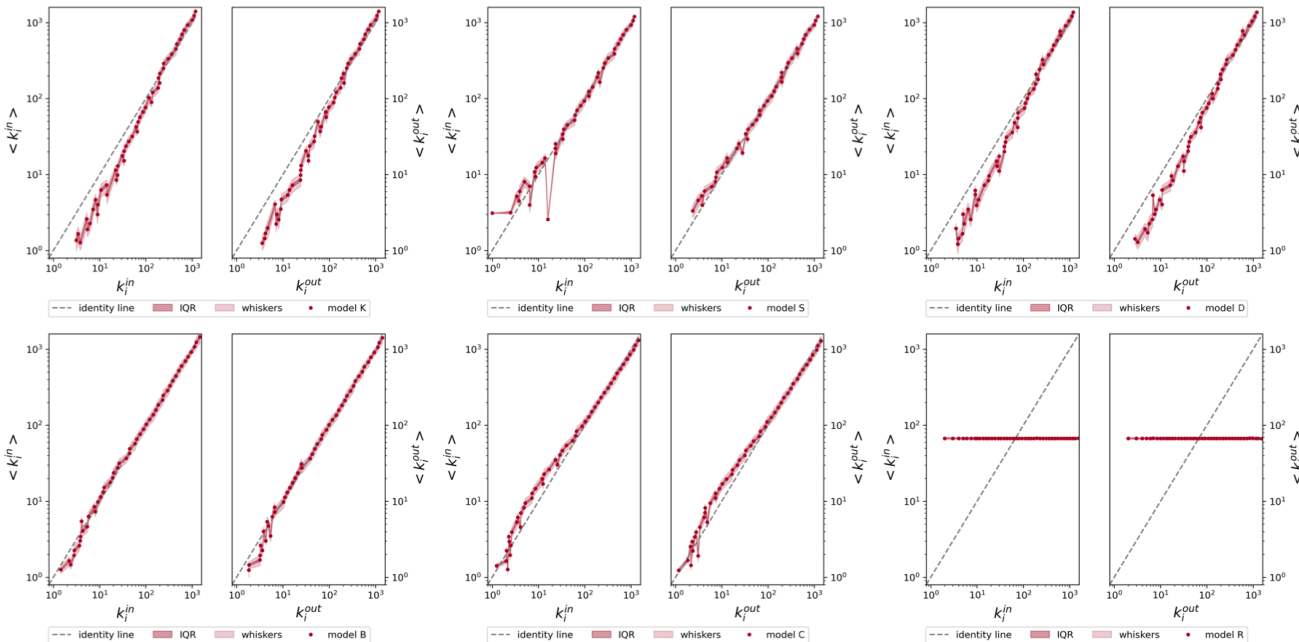


Figure S11. Model in-degrees $\langle k_i^{in} \rangle$ and out-degrees $\langle k_i^{out} \rangle$ versus observed in-degrees k_i^{in} and out-degrees k_i^{out} for the various models (airport dataset).

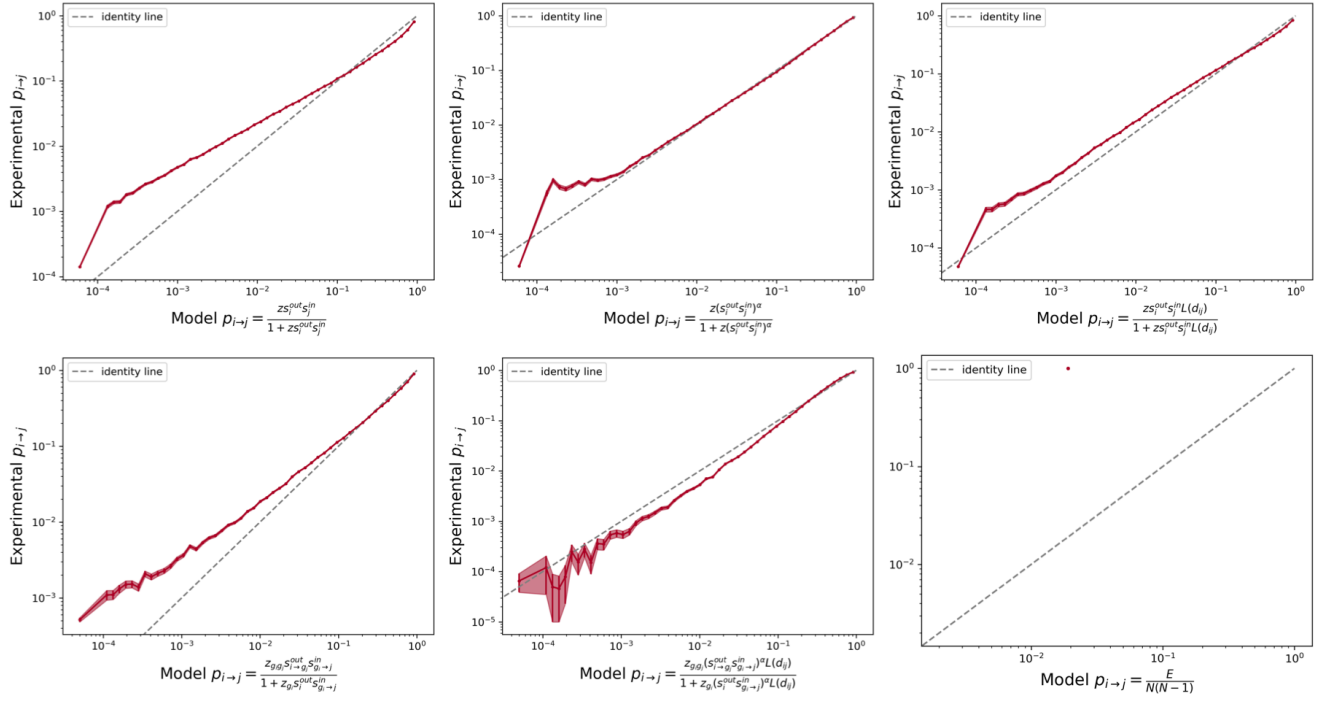


Figure S12. Observed link probability as a function of model link probability for the various models (airport dataset). From top to bottom, and left to right: model K, S, D, B, C, R.

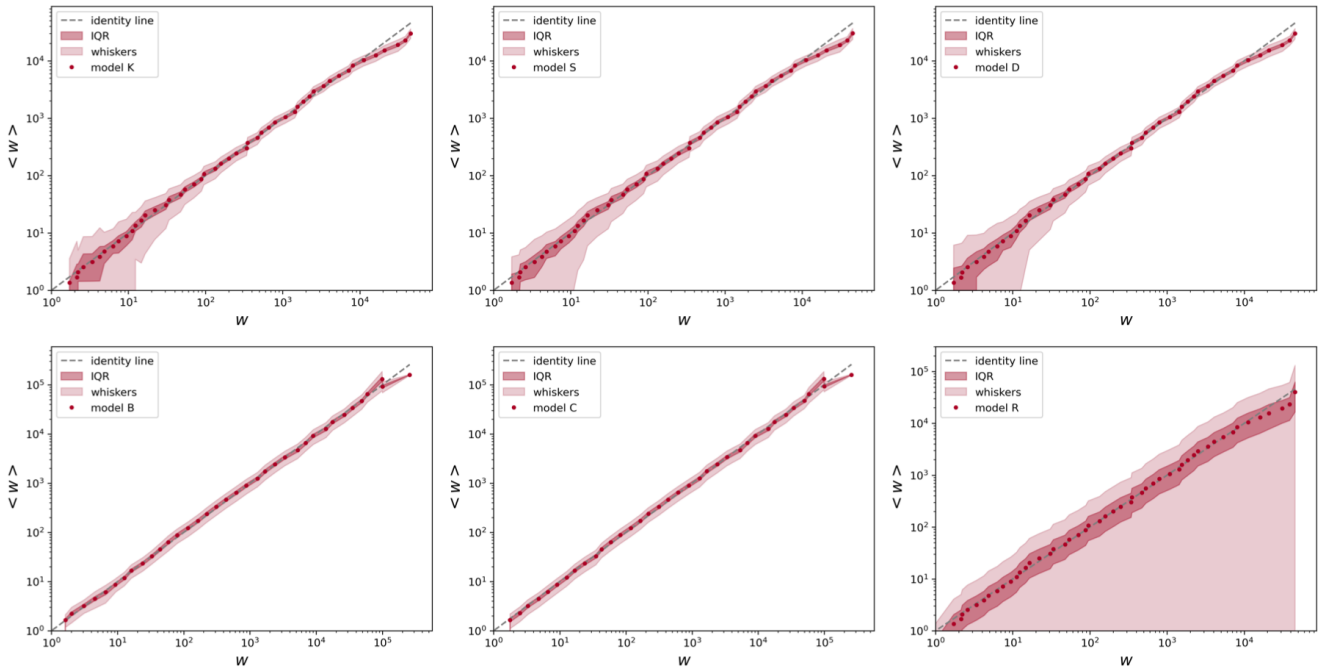


Figure S13. Model weights versus observed weights for the various models (airport dataset).

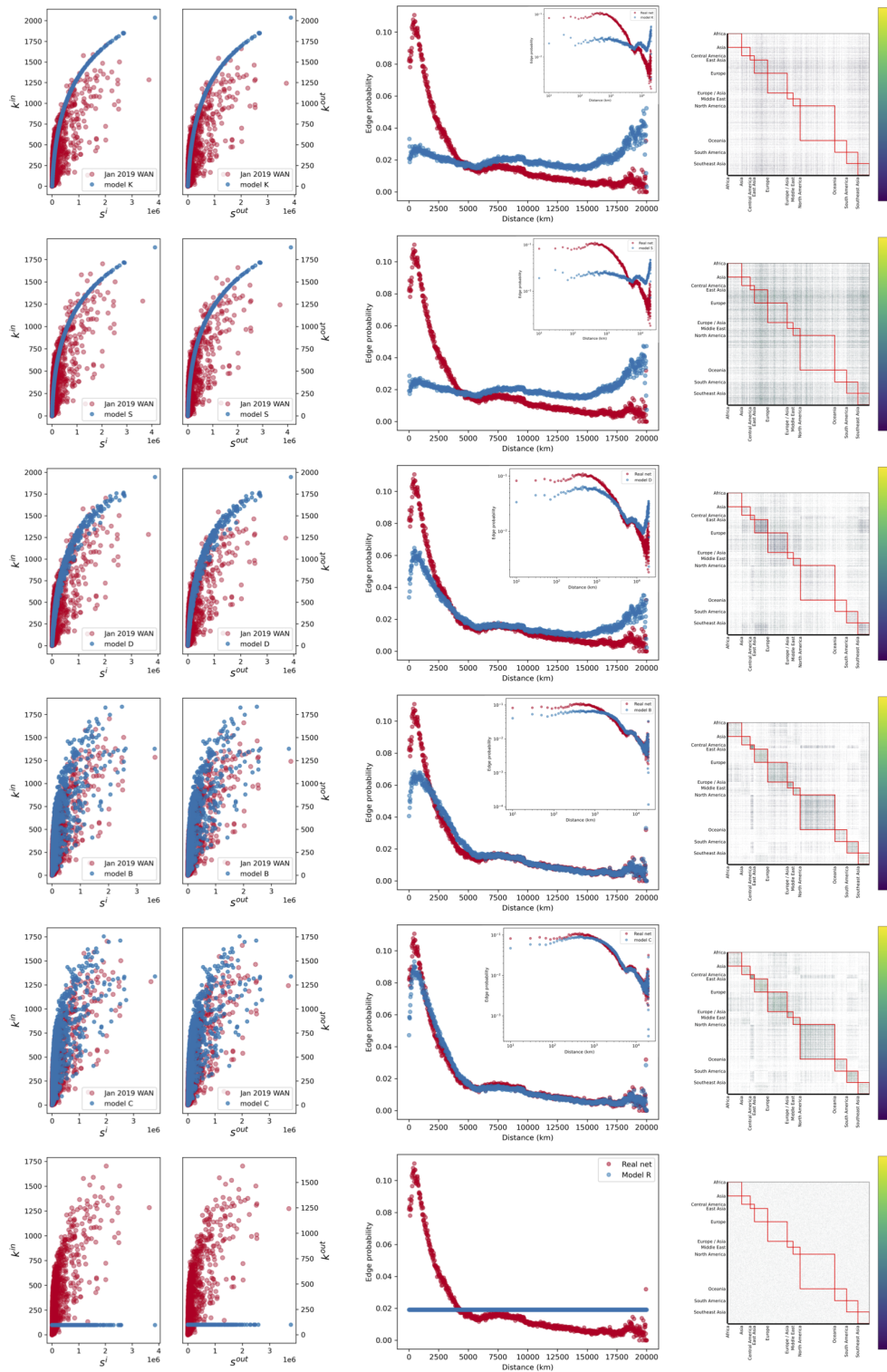


Figure S14. Properties of the model networks for the airport dataset: degree vs strength, edge probability as a function of distance, community structure.